DEUTSCHES ELEKTRONEN-SYNCHROTRON DESY

DESY 80/96
October 1980

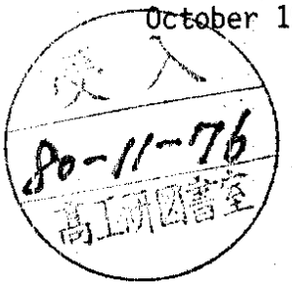

TWO-PHOTON EXCHANGE IN $p^{(-)}p \to \ell^+\ell^- X$ AND A COMPARISON WITH QCD

by

B. Schrempp and F. Schrempp
II. Institut für Theoretische Physik der Universität Hamburg

NOTKESTRASSE 85 · 2 HAMBURG 52

To be sure that your preprints are promptly included in the
HIGH ENERGY PHYSICS INDEX ,
send them to the following address (if possible by air mail) :

DESY
Bibliothek
Notkestrasse 85
2 Hamburg 52
Germany

DESY 80/96
October 1980

TWO-PHOTON EXCHANGE IN $p^{(-)}p \rightarrow e^+e^-X$ AND A COMPARISON WITH QCD

by

B. Schrempp [+] and F. Schrempp [+]

II. Institut für Theoretische Physik
der Universität Hamburg

Presented in part at the International Workshop on $\gamma\gamma$ Collisions,
Amiens, April 8 - 12, 1980.

[+] Heisenberg foundation fellow

Abstract

A thorough study of lepton-pair production from two-photon annihilation in $p^{(-)}p$ collisions is presented. The differential cross section is calculated over a large range of energies ($27 \leq \sqrt{s} \leq 800$ GeV) as a function of the dilepton mass M as well as the dilepton transverse momentum Q_T and the Feynman variable x_F. No kinematical approximations (such as the equivalent photon approximation) are made. For $Q_T \approx 0$ the two-photon mechanism represents an important fraction of the $pp \rightarrow e^+e^-X$ cross section already at ISR energies, whereas at ISABELLE energies it dramatically dominates in the interval $0 \leq Q_T \lesssim 1$ GeV. At ISR energies these conclusions follow from a direct comparison of the two-photon contribution with $pp \rightarrow e^+e^-X$ data. For the ISABELLE energy range the expected $\mathcal{O}(\alpha_s)$QCD contribution to $pp \rightarrow l^+l^-X$, corrected for soft gluon radiation to all orders (in leading bilogarithmic approximation), was taken as a reference. At larger Q_T and ISR energies the $\gamma\gamma$ contribution is negligible, whereas at $\sqrt{s} = 800$ GeV $\gamma\gamma$/QCD $\simeq 10 \div 20$ % almost everywhere. Furthermore, two-photon candidate events from the ISR are shown to be in reasonable agreement with theory. A decomposition of the $\gamma\gamma$ cross section into contributions from both proton vertices being elastic, inelastic and of mixed configuration is given. The results provide important clues for a future isolation of the two-photon mechanism.

1. Introduction

There is increasing theoretical and experimental activity in studying particle production from photon-photon annihilation. Both, the purely electromagnetic subprocess $\gamma\gamma \to l^+l^-$ and the subprocess $\gamma\gamma \to$ hadrons, including $\gamma\gamma \to q$-jet and $\bar{q}$-jet at large transverse momentum, have recently been identified in e^+e^- collisions for the first time [1]. Moreover, first qualitative evidence for two-photon events of the type $pp \to \gamma\gamma X \hookrightarrow \mu^+\mu^-$ has recently been reported [2] from the ISR.

In this paper we shall study in detail the two-photon contribution, $\gamma\gamma \to l^+l^-$, in $p(\bar{p})$ collisions. More specifically, we calculate the two-photon contribution to $p(\bar{p}) \to l^+l^-X$ over a large range of energies as a function of the dilepton mass M as well as the dilepton transverse momentum Q_T and the Feynman variable $x_F = 2Q_L/\sqrt{s}$.

Up to now only calculations of the two-photon contribution integrated over transverse and longitudinal lepton pair momenta, i.e. $d\sigma^{\gamma\gamma}/dM$ (or at best estimates of $d^2\sigma/dMdx_{F/x_F = 0}$) have been available [3-6]. Recently the $O(\alpha^4)$ two-photon contribution to $d\sigma/dM\,(pp \to l^+l^-X)$ has been compared to the $O(\alpha^2)$ Drell-Yan mechanism [5,6]. The $\gamma\gamma$ contribution was found to strongly increase with c.m. energy and to represent a serious competition process to the Drell-Yan mechanism for sufficiently high energies, both for $\tau \equiv M^2/s \ll 1$ and for $\tau \gtrsim 0.25$, say.

Of course, the relative importance of the two-photon mechanism may vary in addition dramatically with Q_T (and x_F). Let us briefly discuss the rough expectations.

For small values of Q_T the two-photon subprocess is expected to show a very steep Q_T distribution, much steeper than the total $pp \to l^+l^-X$ distribution. Thus it seems well possible that the $\gamma\gamma$ mechanism becomes important, if not dominant, at small Q_T (even for values of τ and s where its Q_T integrated contribution is not large).

Recently, arguments have been put forward that perturbative QCD predictions for the lepton pair Q_T distribution remain reliable down to small Q_T, $\Lambda \lesssim Q_T \ll M$, if suitable resummation techniques are used, accounting for

the emission of soft gluons to all orders [7-11]. In such a framework, the peak near $Q_T \approx 0$ is predicted to flatten dramatically (or even show a turnover) with a width proportional to $(M^2/\Lambda^2)^{0.31}$. Therefore, it is clearly important to investigate, whether this characteristic QCD effect is swamped by the two-photon contribution at high energies.

At large Q_T, one expects from dimensional analysis the same power behaviour

$$s\,\frac{d^3\sigma^{\gamma\gamma}}{d\sqrt{\tau}\,dQ_T^2\,dY} \underset{\substack{Q_T \text{ large} \\ \tau,\ Q_T/\sqrt{s},\ Y \text{ fixed}}}{\sim} Q_T^{-2}\, f\left(\tau, \frac{Q_T^2}{s}, Y, \log s\right) \qquad (1)$$

for the two-photon contribution as for the $O(\alpha_s)$ QCD corrections to the Drell-Yan mechanism (involving the subprocess $q\bar{q} \to \gamma$ gluon and gluon + $q \to \gamma q$). However, whereas the $O(\alpha_s)$ QCD contribution [12,13] rather decreases for increasing energies due to logarithmic scaling violations, the two-photon cross section shows a quite dramatic increase like a power of logs.

One might, therefore, well suspect that at very high energies and largish Q_T the two-photon mechanism contributes again at least a sizeable fraction to the lepton-pair cross section.

At the forthcoming very high energy machines (ISABELLE, $\bar{p}p$ collider, ...) there will certainly be measurements of the lepton pair Q_T distribution, taylored to test the predictions of perturbative QCD. Correspondingly, an important issue in this paper is an extensive comparison between the two-photon contribution and predictions of perturbative QCD for $pp \to l^+l^-X$ both at small and large Q_T and high energies $\sqrt{s} \lesssim 800$ GeV.

In summary, the purpose of this paper is to determine the kinematical regions (in all variables M, Q_T, x_F and $\sqrt{s}$), where the two-photon mechanism makes up a sizeable fraction of the differential $p(\bar{p}) \to l^+l^-X$ cross section. We particularly concentrate on Q_T distributions and energies available to the next generation of experiments.

This investigation is useful

i) for estimating a significant two-photon background to perturbative QCD predictions

ii) for a future experimental isolation of the two-photon mechanism as a process of interest in itself

Moreover, let us mention another possibly interesting aspect of this investigation: once the calculational machinery is set up for $\gamma\gamma \to l^+l^-$, one may obtain - with minor modifications - information on signature and rates of events from the subprocesses $\gamma\gamma \to$ q-jet + $\bar{q}$-jet and γ + gluon $\to$ q-jet + $\bar{q}$-jet in $p^{(-)}\bar{p} \to$ 2 jets + X.

The paper is organized as follows. Sect. 2 is devoted to the details of calculation: Subsect. 2.1 contains a short summary of the general formalism for $p^{(-)}\bar{p} \to \gamma\gamma_{e,\mu}\, X$, in Subsect. 2.2 we introduce the socalled 'transverse photon' approximation, Subsect. 2.3 contains the parametrizations used for the elastic and inelastic proton formfactors, in Subsect. 2.4 we specify the QCD prototype calculation used for comparison and Subsect. 2.5 contains some kinematical restrictions, which our external variables have to satisfy. In Sect. 3 we present and discuss our results: Subsect. 3.1 contains information on the numerical calculations and various checks of the results. In Subsect. 3.2 we decompose the $\gamma\gamma$ cross section into contributions from elastic and inelastic proton vertices and point out the dominant configurations in various kinematical regions.
Our results for fixed values of Q_T and M and energies $27 \leq \sqrt{s} \leq 800$ GeV are presented in Subsect. 3.3. The $\gamma\gamma$ mechanism is compared i) with ISR data for $pp \to e^+e^-X$ and $pp \to \gamma_{e,\mu}\gamma_{e,\mu}\, X_{\mu^+\mu^-}$, ii) with our QCD reference cross section for $pp \to l^+l^-X$ with particular emphasis on very high (ISABELLE) energies. Subsect. 3.4 contains our results for fixed $x_T = 2Q_T/\sqrt{s}$ and $\tau = M^2/s \gtrsim 0.1$ and again a comparison with the contribution expected from QCD. In Subsect. 3.5 we briefly discuss the characteristics of the x_F dependence of the $\gamma\gamma$ mechanism. We close with a summary and conclusions in Sect. 4. In an appendix we list the exact expressions for the kinematical boundaries of our four integration variables.

2. Details of calculation

2.1 General formalism

A detailed presentation of the general formalism for the two-photon mechanism in proton-proton (antiproton) collisions

$$p^{(-)}\bar{p} \longrightarrow \gamma\gamma\, X \hookrightarrow l^+l^- \tag{2}$$

may be found in Refs. [3,4]. Here, we shall only summarize the essential steps. Our notation is displayed in Fig. 1, with proton four momenta p_i ($i = 1,2$), virtual (space like) photon four momenta q_i ($q_i^2 = -Q_i^2 < 0$), lepton four momenta k_i, proton mass m and lepton mass μ. Moreover, let

$$Q \equiv k_1 + k_2 = q_1 + q_2 = (Q^0, \vec{Q}_T, Q_L) \tag{3}$$

be the dilepton four momentum with

$$Q^2 = M^2 . \tag{4}$$

All kinematical variables - if not invariant - refer to the overall pp center of mass (c.m.) frame.

The cross section for reaction (2) may be expressed [3,4] - according to the optical theorem - in terms of the absorptive parts of the virtual forward Compton amplitude and of the $\gamma\gamma \to l^+l^- \to \gamma\gamma$ amplitude with l^+l^- intermediate state (Fig. 2):

$$d\sigma = \frac{2m^2}{\sqrt{\lambda(s,m^2,m^2)}} \left(\frac{\alpha}{\pi}\right)^2 \frac{1}{(2\pi)^2} \frac{1}{q_1^4 q_2^4}\, W^{(1)}_{\mu\nu}(-q_1,p_1) \cdot \cdot a^{\nu\nu'\mu\mu'}(q_1,q_2)\, W^{(2)}_{\mu'\nu'}(-q_2,p_2)\, d^4q_1 d^4q_2 \tag{5}$$

where

$$\lambda(x,y,z) = x^2 + y^2 + z^2 - 2xy - 2xz - 2yz . \tag{6}$$

$a^{\nu\nu';\mu\mu'}(q_1, q_2)$ is the absorptive part of the $\gamma\gamma \to l^+l^- \to \gamma\gamma$ amplitude, computable [3,4] in QED

$$a^{\nu\nu';\mu\mu'}(q_1,q_2) = \sum_{\text{lepton spins}} \int \frac{d^3k_1}{(2\pi)^3} \frac{d^3k_2}{(2\pi)^3} \frac{\mu^2}{k_1^0 k_2^0} (2\pi)^4 \cdot \delta^4(k_1+k_2-q_1-q_2)\, T^{\nu\mu'}(\gamma\gamma\to l^+l^-)\, T^{\nu\nu'*}(\gamma\gamma\to l^+l^-) \tag{7}$$

and $W^{(i)}_{\mu\nu}$ is the absorptive part of the forward (proton) Compton amplitude with standard decomposition into invariant structure functions W_1 and W_2

$$W^{(i)}_{\mu\nu}(-q_i, p_i) = -W_1^{(i)}(x_i, Q_i^2)\left(g_{\mu\nu} - \frac{q_{i\mu}q_{i\nu}}{q_i^2}\right) + \frac{W_2^{(i)}(x_i,Q_i^2)}{m^2}\left(p_{i\mu} - \frac{q_{i\mu}\,q_i p_i}{q_i^2}\right)\left(p_{i\nu} - \frac{q_{i\nu}\,q_i p_i}{q_i^2}\right) \tag{8}$$

involving the Bjorken scaling variables

$$x_i = -\frac{q_i^2}{2\,q_i p_i} = \frac{Q_i^2}{2 q_i p_i} \qquad i=1,2. \tag{9}$$

It is convenient [3,4] to evaluate Eq. (5) in terms of helicity amplitudes defined in the $\gamma\gamma$ c.m.-system. The helicity projections of the amplitudes take the standard form in terms of photon polarization vectors $\varepsilon^{\mu}_{\lambda}(q)$

$$a_{\lambda_3\lambda_4;\lambda_1\lambda_2}(q_1^2, q_2^2, M^2) = \varepsilon^{\nu*}_{\lambda_3}(q_1)\,\varepsilon^{\nu'*}_{\lambda_4}(q_2)\,\varepsilon^{\mu}_{\lambda_1}(q_1)\,\varepsilon^{\mu'}_{\lambda_2}(q_2)\cdot a_{\nu\nu';\mu\mu'}(q_1,q_2) \tag{10}$$

The helicity projections of the tensor $W^{(i)}_{\mu\nu}$ are defined analogously.

The polarization vectors fulfill the standard orthogonality and completeness relations

$$\varepsilon^{\mu}_{m}(q)\,\varepsilon^{\nu}_{m'}(q)\,g_{\mu\nu} = (-1)^m \delta_{mm'}$$

$$\sum_m (-1)^m \varepsilon^{\mu}_m(q)\,\varepsilon^{\nu}_m(q) = g^{\mu\nu} - q^\mu q^\nu/q^2 \tag{11}$$

$$q^\nu\,\varepsilon^{\mu}_m(q)\,g_{\mu\nu} = 0.$$

By P and T invariance there remain eight independent $\gamma\gamma$ helicity amplitudes or equivalently $\gamma\gamma$ cross sections σ_{ab} for transverse (a,b = T $\hat{=}$ $\lambda = \pm 1$) and scalar (a,b = S $\hat{=}$ $\lambda = 0$) photon polarization and interferences (τ_{ab}) thereof. They are given e.g. in Ref. [4]. For our case of unpolarized protons only six $\gamma\gamma$ cross sections occur. In particular, for $|q_i^2| \ll Q^2 \equiv M^2$ the dominant $\gamma\gamma$ cross section is [4]

$$\begin{aligned}\sigma_{TT}(M^2,q_1^2,q_2^2) &= (a_{11;11} + a_{1-1;1-1})\big/\left(4\sqrt{\lambda(M^2,q_1^2,q_2^2)}\right)\\ &= \frac{4\pi\alpha^2}{\lambda(M^2,q_1^2,q_2^2)}\Bigg[\frac{1}{2}(M^2-q_1^2-q_2^2)\cdot L\cdot\Big\{2+\frac{2\mu^2}{x} - \Big(\frac{2\mu^2}{q_1 q_2}\Big)^2 + \frac{q_1^2+q_2^2}{x} + \frac{q_1^2 q_2^2 M^2}{2x(q_1q_2)^2} + \frac{3}{4}\Big(\frac{q_1^2q_2^2}{x(q_1q_2)}\Big)^2\Big\}\\ &\quad - \Delta t\Big\{1+\frac{\mu^2}{x} + \frac{q_1^2+q_2^2}{x} + \frac{q_1^2q_2^2}{4x\mu^2+q_1^2q_2^2} + \frac{3}{4}\frac{q_1^2q_2^2}{x^2}\Big\}\Bigg]\\ &= \frac{4\pi\alpha^2}{M^2}\,\sigma(L)\end{aligned} \tag{12}$$

with

$$M^2 x = (q_1q_2)^2 - q_1^2q_2^2 = \lambda(M^2,q_1^2,q_2^2)/4 \tag{13}$$

$$\Delta t = t_{max} - t_{min} = \sqrt{4x\,(M^2-4\mu^2)} \tag{14}$$

and

$$L = \ln\frac{\mu^2 - t_{min}}{\mu^2 - t_{max}} = \ln\frac{(M^2-q_1^2-q_2^2+\Delta t)^2}{4\,(q_1^2q_2^2 + 4x\mu^2)} \tag{15}$$

The other $\gamma\gamma$ cross sections behave as [4]

$$\tau_{TT} = \frac{4\pi\alpha^2}{M^2}\,\sigma\left(L\,\frac{q_1^2 q_2^2}{M^4}\right),$$

$$\sigma_{TS} = \frac{4\pi\alpha^2}{M^2}\,\sigma\left(-\frac{q_2^2}{M^2}\right),\quad \sigma_{ST} = \frac{4\pi\alpha^2}{M^2}\,\sigma\left(-\frac{q_1^2}{M^2}\right)$$

$$\tau_{TS} = \frac{4\pi\alpha^2}{M^2}\,\sigma\left(\frac{\sqrt{q_1^2 q_2^2}}{M^2}\right),\quad \sigma_{SS} = \frac{4\pi\alpha^2}{M^2}\,\sigma\left(L\,\frac{q_1^2 q_2^2}{M^4}\right). \qquad (16)$$

For $|q_i^2| < M^2$ the quantities (16) are negligibly small [4] in comparison with σ_{TT}, but in σ_{TT} the q_i^2-dependence is essential in the large domain $M^2\mu^2 < q_1^2 q_2^2 < M^4$.

As outlined in the introduction, we are interested in the differential cross section $d^3\sigma/dM^2 dQ_T^2 dY$ with Y being the lepton-pair rapidity in the pp cms, defined as

$$Y = \frac{1}{2}\ln\frac{Q^0 + Q_L}{Q^0 - Q_L} \qquad (17)$$

and related to Feynman $-x_F$ by

$$x_F = \frac{2Q_L}{\sqrt{s}} = \frac{2\sqrt{M^2+Q_T^2}}{\sqrt{s}}\sinh Y. \qquad (18)$$

Furthermore

$$Q^0 = q_1^0 + q_2^0 = \sqrt{M^2+Q_T^2}\,\cosh Y. \qquad (19)$$

A straight forward calculation leads to the Jacobian relation

$$\frac{d^4q_1\,d^4q_2}{(q_1^2)^2(q_2^2)^2} = \frac{s}{4\lambda(s,m^2,m^2)}\,\frac{2\pi}{4\sqrt{-\lambda(Q_T^2,|\vec{q}_{1T}|^2,|\vec{q}_{2T}|^2)}}$$
$$\cdot dM^2 dQ_T^2 dY\,\frac{dx_1}{x_1^2}\,\frac{dx_2}{x_2^2}\,\frac{dQ_1^2}{Q_1^2}\,\frac{dQ_2^2}{Q_2^2}; \qquad (20)$$

where one trivial azimuthal integration has already been performed. The Bjorken variables are defined in (9) and $-q_i^2 = Q_i^2$. Obviously, four integrations have to be performed in Eq. (5) in order to calculate $d^3\sigma/dM^2\,dQ_T^2 dY$. Let us remark that the O(2,1) variables used in Ref. [3] for a calculation of $d\sigma/dM^2$ are not so advantageous here.

The kinematical boundaries for the four integration variables x_i and Q_i^2, $i = 1,2$, are obtained as follows.

First, the range of the integration variable Q_2^2 as a function of Q_1^2, x_1 and x_2 is restricted from

$$-\lambda(Q_T^2,|\vec{q}_{1T}|^2,|\vec{q}_{2T}|^2) \equiv (Q_T^2 - (|\vec{q}_{1T}| - |\vec{q}_{2T}|)^2)\cdot (-Q_T^2 + (|\vec{q}_{1T}| + |\vec{q}_{2T}|)^2) \geq 0 \qquad (21)$$

in order to keep $\sqrt{-\lambda}$ real in Eq. (20). The r.h.s. of Eq. (21) depends on Q_2^2 quadratically (see appendix). Thus, $Q_2^2{}_{\substack{\max\\\min}}(Q_1^2, x_1, x_2)$ is obtained as solution of the equation $\lambda = 0$ in the form

$$Q_2^2{}_{\substack{\max\\\min}} = \frac{x_2}{2a}\left(-b \pm \sqrt{b^2-4ac}\right) \qquad (22)$$

with a, b and c given in the appendix.

The range of the integration variable Q_1^2 as a function of x_1 and x_2 is then restricted by the condition

$$b^2 - 4ac \geq 0. \qquad (23)$$

Thus $Q_1^2{}_{\substack{\max\\\min}}(x_1, x_2)$ is obtained as solution of the equation $b^2-4ac = 0$ in the form

$$Q_1^2{}_{\substack{\max\\\min}} = \frac{x_1}{2A}\left(-B \mp \sqrt{B^2-4AC}\right) \qquad (24)$$

with A, B and C given in the appendix.

Similarly $x_{1,min}(x_2)$ is determined from the roots of the limiting equation $B^2 - 4AC = 0$ (see appendix) and

$$x_{1,max} = 1 .$$

Finally $x_{2,min} = x_{1,min}$ ($Y \to -Y$, $x_2 = 1$) (25)

and

$$x_{2,max} = 1 . \qquad (26)$$

2.2 The transverse approximation

Usually, in two-photon physics, the socalled equivalent photon approximation (EPA) is applied [4,5], effecting great simplification. The essence of the EPA consists of

i) treating the two photons on-shell ($q_i^2 \simeq 0$) and

ii) retaining only transverse photon polarization.

As a result of i) and ii) the cross section factorizes into a product of a $\gamma\gamma$ cross section and "flux factors" from the equivalent photon spectra produced by the colliding particles.

Unfortunately approximation i) is not suitable for our purposes. Since we are interested in a kinematical region where both

$$(q_1 + q_2)^2 = Q^2 = M^2$$

and (27)

$$(\vec{q}_{1T} + \vec{q}_{2T})^2 = Q_T^2$$

are large, we must certainly go beyond i) of the EPA. (c.f. also appendix, Eqs. (A8, A12)).

In view of Eqs. (16) also condition ii) of the EPA becomes doubtful for large Q_T. In principle one ought to take into account all $\gamma\gamma$ cross sections, to treat the q_i^2 dependences in Eqs. (12,16) exactly and to perform the q_i^2 integrations. However, in order to keep computing efforts within reasonable limits, in this investigation we have taken into account the transverse $\gamma\gamma$ cross section σ_{TT} only. Because of the numerical smallness [4] of the neglected cross sections relative to σ_{TT} for $|\eta_i|^2/M^2 \lesssim 1$ our results should be quite accurate for not too large Q_T^2/M^2. At very large values of Q_T they should at least represent an order of magnitude estimate in the sense of a lower bound for the $\gamma\gamma$ contribution.

The important point is, that we calculate σ_{TT} exactly (Eq. (12)), i.e. we retain the full q_i^2 dependences and perform the q_i^2 integrations explicitly.

Moreover, let us point out an important technical detail: one has to be very careful when making approximations in the expressions for the integration limits (see appendix). For large Q_T significant contributions come from close to the kinematical boundaries of the integration variables. Even neglecting nucleon mass effects in the integration limits may lead to negative cross sections. The present calculation has been performed with the exact expressions for the integration limits, given in the appendix.

With the transverse approximation specified above and the Jacobian relation (20) the cross section (5) takes the following form

$$\frac{d^3\sigma^{transv.}}{dM^2 dQ_T^2 dY}\left(P\bar{P}^{(-)} \to \gamma\gamma \underset{\hookrightarrow \ell^+\ell^-}{X}\right) = \left(\frac{\alpha^2}{\pi}\right)^2 \frac{1}{s^2} \int_{x_{2,min}}^{1} \frac{dx_2}{x_2^2} \int_{x_{1,min}}^{1} \frac{dx_1}{x_1^2}$$

$$\int_{Q_{1,min}^2}^{Q_{1,max}^2} \frac{dQ_1^2}{Q_1^2} \int_{Q_{2,min}^2}^{Q_{2,max}^2} \frac{dQ_2^2}{Q_2^2} \frac{x_2}{\sqrt{\left(u_2^2 + \frac{m^2}{s-4m^2} x_T^2\right)(Q_2^2 - Q_{2,min}^2)(Q_{2,max}^2 - Q_2^2)}} \qquad (28)$$

$$W_{++}^{(1)} \frac{\sigma_{TT}\sqrt{\lambda(M^2, Q_1^2, Q_2^2)}}{4\pi\alpha^2} W_{++}^{(2)}$$

with [1]

$$W_{++} = 2m W_1(x_1, Q_1^2) + \frac{\nu W_2(x_1, Q_1^2)}{x_1}\left[\frac{2}{\lambda(M^2, Q_1^2, Q_2^2)} \cdot \{(sx_1\xi_1 + Q_1^2)(sx_1\xi_1 - M^2) - sx_1\xi_1 Q_2^2\} - \frac{2m^2 x_1^2}{Q_1^2}\right] \qquad (29)$$

$$W_{++}^{(2)} = W_{++}^{(1)}(x \leftrightarrow x_2, Q_1^2 \leftrightarrow Q_2^2, \xi_1 \leftrightarrow \xi_2)$$

where σ_{TT} is given in Eq. (12), the integration limits in the appendix and

$$x_T = \frac{2Q_T}{\sqrt{s}}\ , \quad \tau = \frac{M^2}{s}\ , \quad \bar{x}_T = \sqrt{4\tau + x_T^2} \tag{30}$$

$$\xi_{1,2} = \frac{\bar{x}_T}{2}\left(\cosh Y \mp \sqrt{\frac{s-4m^2}{s}}\sinh Y\right) \text{ and} \tag{31}$$

$$u_{1,2} = x_{1,2} - \tfrac{1}{2}\bar{x}_T\left(\cosh Y \pm \sqrt{\frac{s}{s-4m^2}}\sinh Y\right). \tag{32}$$

Moreover in Eq. (28)

$$\sqrt{\frac{(u_2^2 + \frac{m^2}{s-4m^2}x_T^2)}{x_2^2}(Q_2^2 - Q_{2,\min}^2)(Q_2^2 - Q_{2,\max}^2)} = \sqrt{-\lambda(Q_T^2, |\vec{q}_{1T}|^2, |\vec{q}_{2T}|^2)} \tag{33}$$

We recall that Eq. (28) does not contain any approximations so far apart from the "transverse" one.

2.3 Structure functions

The proton structure functions $2mW_1$ and νW_2 represent the second building block besides the $\gamma\gamma$ helicity amplitudes, entering the $pp \to \gamma\gamma X \to \ell\ell$ cross section.

The elastic contribution reads [3,4]

$$2mW_1(x,Q^2) \Longrightarrow \delta(x-1)\, G_M^2(Q^2) \tag{34}$$

$$\nu W_2(x,Q^2) \Longrightarrow \delta(x-1)\left(G_E^2(Q^2) + \frac{Q^2}{4m^2}G_M^2(Q^2)\right)\Big/\left(1+Q^2/4m^2\right)$$

where G_E and G_M are the usual electric and magnetic proton form factors and have the normalization $G_E(0) = 1$ and $G_M(0) = \mu_p$, with proton magnetic moment $\mu_p = 2.79$. In our calculations we use the standard dipole fit

$$G_E(Q^2) = \frac{G_M(Q^2)}{\mu_p} = \left(1 + \frac{Q^2}{m_0^2}\right)^{-2}\ ; \quad m_0^2 = 0.71\ \text{GeV}^2 \tag{35}$$

For the inelastic structure functions $2mW_1$ and νW_2 one may use in principle directly the experimental data as functions of x_i and Q_i^2. For simplicity, however, we adopt for νW_2 the parametrization of Bloom and Gilman [14] in terms of the variable

$$\omega_i' = \frac{1}{x_i} + \frac{m^2}{Q_i^2}$$

$$\nu W_2 = .557\,(1-\tfrac{1}{\omega'})^3 + 2.1978\,(1-\tfrac{1}{\omega'})^4 - 2.5954\,(1-\tfrac{1}{\omega'})^5 \tag{36}$$

together with a more recent fit by G. Fox [15] for

$$R = \frac{\nu W_2}{2mx\,W_1}\left(1 + \frac{4m^2x^2}{Q^2}\right) - 1 = \frac{0.861\,Q^2}{(Q^2+.988)^2}$$

[with Q^2 in GeV^2]. (37)

This parametrization obviously ignores the resonance fluctuations present in the data. However, since only integrals over the structure functions of the form

$$\int \frac{dQ^2}{Q^2}\int \frac{dx}{x^2}\left\{\begin{matrix} 2m\,W_1(x,Q^2) \\ \nu\,W_2(x,Q^2)\end{matrix}\right\} \tag{38}$$

appear in Eq. (28), one may qualitatively invoke duality arguments [16] to argue that these fluctuations probably will wash out in the integrals and that parametrization (36,37) may thus be used right down to the inelastic threshold to good approximation.

The inelastic threshold condition

$$(p_i - q_i)^2 \geq (m + m_{\pi^0})^2 \tag{39}$$

gives the constraint (for $x_i \to 1$)

$$Q_i^2 \geq \frac{x_i}{1-x_i}\left[(m+m_{\pi^0})^2 - m^2\right] \simeq 0.27\,\mathrm{GeV}^2\,\frac{x_i}{1-x_i} \tag{40}$$

which was built into our calculation.

In fact, one easily finds that the minimal Q_i^2 for inelastic scattering in Eq. (40) increases † with Q_T^2 and hence, for large enough Q_T^2, the resonance fluctuations should not matter anyway.

For small Q_T and M we follows Ref. [3] and multiply νW_2 in Eq. (36) with a correction factor

$$\nu W_2^{(i)} \longrightarrow \nu W_2^{(i)}\; Q_i^2/(Q_i^2 + 0.15\,\mathrm{GeV}^2) \tag{41}$$

in order to restore the gauge invariance condition

$$W_2^{(i)}\Big|_{Q_i^2=0} = 0 \tag{42}$$

and to match on to the observed real photoabsorption cross section $\sigma_{\gamma p}$ at $Q_i^2 = 0$.

2.4 QCD prototype for $pp \longrightarrow l^+l^-X$

In order to assess the relative importance of the two-photon contribution in various regions of phase space, a suitable reference cross section is needed. Experimental data on $pp \longrightarrow l^+l^-X$ from FNAL are, at present, limited [17-19] to $\sqrt{s} \lesssim 27.3$ GeV, $Q_T \lesssim 3.5$ GeV and $M \lesssim 12$ GeV and those from the ISR to $\sqrt{s} \lesssim 63$ GeV, $Q_T \lesssim 6$ GeV and $M \lesssim 20$ GeV. At small Q_T and ISR energies a direct comparison of our differential two-photon distributions with representative ISR data is performed in Subsect. 3.3.

For the discussion of our two-photon results in other kinematical regions - in particular at ISABELLE energies - we take simple, perturbative QCD estimates for $pp \longrightarrow l^+l^-X$ as a reference.

For $Q_T = \sigma(M) \gg \Lambda$ the $\sigma(\alpha_s)$ corrections to the Drell-Yan mechanism, i.e. the subprocesses

$$q\bar{q} \longrightarrow \gamma^* + \text{gluon} \quad \text{and} \quad \text{gluon} + q \longrightarrow \gamma^* + q \tag{43}$$

($\gamma^* \hookrightarrow l^+l^-$ in both cases)

may be expected to represent the dominant QCD contributions to the dilepton Q_T distribution. The corresponding cross sections $d\sigma^{QCD}/dM^2 dQ_T^2 dY$ have been calculated by various authors [12,13] and qualitatively argree with existing experimental data for a reasonable value of the running coupling constant [12]

$$\langle \alpha_s \rangle \simeq 0.3 \tag{44}$$

over the mass range $5 \leq M \leq 10$ GeV.

The calculation by Kajantie and Raitio [12] represents a simple prototype and we have chosen to take it as a QCD reference for our $\gamma\gamma$ results in the region $Q_T = \sigma(M) \gg \Lambda$. The $\sigma(\alpha_s)$ QCD expressions to be used read as follows [12]

$$s\,\frac{d^3\sigma(q\bar{q}\to\gamma^* g)}{d\sqrt{\tau}\,dQ_T^2\,dY} = \frac{8}{3}\,\frac{\pi\alpha^2}{(\sqrt{\tau})^3}\,\frac{\alpha_s(s\tau)}{2\pi}\,\frac{4}{9}\,\frac{\tau}{Q_T^2}\cdot$$
$$\cdot \int_{x_{1,\min}}^{1} \frac{dx_1}{x_1 x_2} \sum_{i=1}^{f} e_i^2 \left[F_i(x_1)\,\bar{F}_i(x_2) + (1 \leftrightarrow 2)\right] \cdot \tag{45}$$
$$\cdot\; \frac{1 + \tau^2/(x_1x_2)^2 - x_T^2/(2x_1x_2)}{x_1 - \frac{1}{2}\bar{x}_T e^{Y}}$$

and

† e.g. for $x_F = 0$ this follows from using (see appendix) $x_i/(1-x_i) \geq x_{2,\min}/(1-x_{2,\min}) = (\frac{1}{2}\bar{x}_T - \tau)/(1-\bar{x}_T + \tau - \frac{4m^2}{s})$ (with $\bar{x}_T^2 = 4\tau + x_T^2$) in Eq. (40).

$$s\,\frac{d^3\sigma(qg\to q\gamma^*)}{d\sqrt{\tau}\,dQ_T^2\,dY} = \frac{8}{3}\,\frac{\pi\alpha^2}{(\sqrt{\tau})^3}\,\frac{\alpha_s(s\tau)}{2\pi}\,\frac{1}{3}\,\frac{\tau}{Q_T^2}\cdot$$

$$\int_{x_{1,min}}^{1}\frac{dx_1\,(x_T/2)^2}{(x_1-\frac{1}{2}\bar{x}_T e^{Y})(x_1x_2)^3}\sum_{i=1}^{f}e_i^2\Big[F_i^{(1)}(x_1)\,G^{(2)}(x_2)\cdot \qquad (46)$$

$$\cdot\frac{(x_1x_2-\tau)^2+\frac{1}{4}(x_1x_2+\tau+V)^2}{x_1x_2-\tau+V}+(1\leftrightarrow 2, V\leftrightarrow -V)\Big]$$

where

$$x_2 = \frac{\frac{1}{2}\bar{x}_T e^{-Y}x_1-\tau}{x_1-\frac{1}{2}\bar{x}_T e^{Y}}\,,\qquad x_{1,min} = \frac{\frac{1}{2}\bar{x}_T e^{Y}-\tau}{1-\frac{1}{2}\bar{x}_T e^{-Y}}$$

$$V = \Big\{(x_1x_2-\tfrac{1}{4}(x_T+\bar{x}_T)^2)(x_1x_2-\tfrac{1}{4}(x_T-\bar{x}_T)^2)\Big\}^{1/2}. \qquad (47)$$

Moreover, simple quark (F_i) and gluon (G) distributions have been used in Ref. [12]:

$$\begin{aligned}&\text{valence: } V(x) = \tfrac{35}{32}\sqrt{x}\,(1-x)^3\\ &\text{sea}\quad\ : S(x) = 0.15\,(1-x)^7\\ &\text{glue}\quad : G(x) = \langle x_g\rangle\,(g+1)\,(1-x)^g \qquad g = 7\\ &\qquad\qquad\qquad\qquad \langle x_g\rangle = .56\end{aligned} \qquad (48)$$

The exponents 3 and 7 in Eq. (48) follow from counting rules, V(x) is normalized to 1 when integrated over dx/x, the factor 0.15 in S(x) was determined from neutrino data and $\langle x_g\rangle = 0.56$ from energy momentum sum rules. It should be kept in mind, however, that the gluon distribution G(x), in particular, is not very well known and hence introduces considerable uncertainties for large τ.

Instead of working with a fixed value of $\langle\alpha_s\rangle = 0.3$ - as is done in Ref. [12] - we have taken instead

$$\alpha_s = \alpha_s(s\tau) \equiv \alpha_s(M^2) \simeq \frac{4\pi}{\beta_0\,\ln\frac{M^2}{\Lambda^2}} \qquad (49)$$

with

$$\alpha_s(M^2=1\,GeV^2) = 1 \quad \text{i.e.}\quad \Lambda \simeq 0.5 \qquad (50)$$

leading to

$$\alpha_s(5.5\,GeV^2) = 0.3. \qquad (51)$$

As pointed out already in Ref. 12 the argument of α_s is of course ambiguous.

We recall that the above $\mathcal{O}(\alpha_s)$ QCD expression is formally valid only for $Q_T \sim M \gg \Lambda$. It would clearly be desireable to also have a reliable reference cross section in the region $Q_T \ll M$, $\sqrt{s}$ large, since there the most sizeable manifestation of the two-photon mechanism is expected.

Starting with the work of DDT [7] arguments have been put forward that this region of Q_T may still remain accessible to (suitably resummed) perturbative QCD, provided that

$$\Lambda \lesssim Q_T \ll M \quad \text{and} \quad \sqrt{s}\ \text{large}. \qquad (52)$$

In this region (52) the leading single logarithmic approximation $[\sim\alpha_s^n\ln^n M^2]$ breaks down, since in addition large logarithms $\sim\ln\frac{M^2}{Q_T^2}$ appear.

However, several analyses [8-11] have recently suggested that - analoguously to QED - the sum to all orders of both real and virtual gluon emission simply exponentiates to leading double-logarithmic approximation. Qualitatively, in Q_T space, this results [8-11] in a "quark formfactor"

$$F_q(M^2,Q_T^2) \simeq \exp\Big\{-\int_{Q_T^2}^{M^2}dk_T^2\Big[\frac{d^3\sigma}{dk_T^2\,dM\,dY}\Big|_{Y=0}\Big/\frac{d^2\sigma}{dM\,dY}\Big|_{Y=0}^{(order\,\alpha_s)}\Big\} \qquad (53)$$

$$\simeq \exp\Big\{-\frac{16}{25}\ln\frac{M^2}{\Lambda^2}\ln\Big(\frac{\ln\frac{M^2}{\Lambda^2}}{\ln\frac{Q_T^2}{\Lambda^2}}\Big)+\frac{16}{25}\ln\frac{M^2}{Q_T^2}\Big\} \qquad (54)$$

producing a strong damping (if not a turnover, as implied in approximation (54)) of the $\mathcal{O}(\alpha_s)$ Q_T distribution [8]

$$M^3 \frac{d^3\sigma}{dM\,dQ_T^2\,dY}\Big|_{Y=0} \simeq M^3 \frac{d^2\sigma(\tau)}{dM\,dY}\Big|_{Y=0} \frac{d}{dQ_T^2} F_q(M^2, Q_T^2) \qquad (55)$$

at small $Q_T \gtrsim \Lambda$.

The exponentiation of the $\mathcal{O}(\alpha_s)$ result presents the advantage of being automatically in agreement with the lowest-order calculation when $Q_T \sim M$. Moreover, a characteristic prediction is that the peak near $Q_T \simeq 0$ flattens [8] with a width proportional to $(M^2/\Lambda^2)^{0.31}$.

As a reference for our two-photon results in the region $\Lambda \lesssim Q_T \ll M$, $\sqrt{s}$ large, we take the shape of the Q_T distribution as given by Parisi and Petronzio [8] for ISABELLE energies and $M^2 = 120$, 7500 GeV^2.
It is a somewhat refined version of Eq. (55), with exponentiation applied in impact parameter space and an intrinsic parton transverse momentum $\langle Q_T^2 \rangle_{intr.} \simeq 0.4$ GeV^2 accounted for [the effect of which turns out, however, to be unimportant [8] at ISABELLE energies and $Q_T \gtrsim 0.3$ GeV].

We fix in addition the absolute normalization of the unnormalized Q_T distributions $dN/dM dQ_T^2 dY\,/_{Y=0}$ given in Ref. 8 as follows:

We normalize them for larger $Q_T \gtrsim$ 2-4 GeV to the $\mathcal{O}(\alpha_s)$ calculation of Kajantie and Raitio [12], Eqs. (45), (46), (48), since there the two shapes turn out to agree nicely (see Fig. 9). This way the two QCD expressions used are consistent with each other. As a check for our normalization we extract the corresponding integrated cross section $M^3\, d^2\sigma/dM dY\,/_{Y=0}$

i) by integrating the normalized Q_T distribution of Ref. [8] directly over Q_T^2

and ii) by fitting it to the approximate Eqs (54), (55) at larger Q_T.

Both methods agree within $\lesssim$ 10 % and give

$$M^3 \frac{d^2\sigma^{QCD}}{dM\,dY}\Big|_{Y=0} = \begin{cases} 8.4\ \text{nb}\cdot\text{GeV}^2 \text{ for } M^2 = 120\ \text{GeV}^2 \\ 3.4\ \text{nb}\cdot\text{GeV}^2 \text{ for } M^2 = 7500\ \text{GeV}^2 \end{cases}$$
$$\text{and } \sqrt{s} = 800\ \text{GeV} \qquad (56)$$

in qualitative agreement with experimental data [17-21] from FNAL and ISR for $\sqrt{\tau} \simeq 0.014$ and $\sqrt{\tau} \simeq 0.11$.

2.5 Kinematical restrictions

In this subsection we list some kinematical restrictions, which our external variables

$$\tau = \frac{M^2}{s}, \quad x_F = \frac{2Q_L}{\sqrt{s}} \text{ and } \quad x_T = \frac{2Q_T}{\sqrt{s}} \qquad (57)$$

have to satisfy.

The fractional dilepton energy in the pp c.m. system reads

$$\frac{2Q^0}{\sqrt{s}} = \{ 4\tau + x_F^2 + x_T^2 \}^{1/2} = 1 + \tau - \frac{m'^2}{s} \qquad (58)$$

where m' is the total mass recoiling against the lepton pair. From the threshold restriction $m'^2 \gtrsim 4m^2$ we obtain from Eq. (58)

$$|x_F| \lesssim \sqrt{(1+\tau-\tfrac{4m^2}{s})^2 - 4\tau - x_T^2}$$
$$\underset{s\to\infty}{\simeq} \sqrt{(1-\tau)^2 - x_T^2} \qquad (59)$$

and

$$x_T \lesssim 1-\tau. \qquad (60)$$

Therefore, in order to minimize effects due to the kinematical boundaries when displaying our results, we shall sometimes use the reduced variables

$$0 \leq \hat{x}_F \equiv \frac{Q_L}{Q_{L,max}} \simeq \frac{x_F}{\sqrt{(1-\tau)^2 - x_T^2\,\tau}} \leq 1 \qquad (61)$$

$$0 \leq \hat{x}_T \equiv \frac{Q_T}{Q_{T,max}} \simeq \frac{x_T}{1-\tau} \leq 1 \qquad (62)$$

besides

$$0 \leq \tau = \frac{M^2}{s} \leq 1 . \qquad (63).$$

3. RESULTS

3.1 Numerical evaluation and checks

The four integrations in Eq. (28) have been performed numerically with a Gauss-type integration method. A relative accuracy of 10 % was required in every integration. A Monte Carlo method has also been tried, but - surprisingly - turned out to be more time consuming than the Gauss method †. Considerable effort was spent to obtain an estimate of the results in analytical form as well. This attempt remained, however, unsuccessful, since the dominant portion of the integration region turned out to depend on the external variables in a complicated way.

We have performed - among others - the following quantitative checks with our numerical results:

i) the differential cross section $d^3\sigma/dMdQ_T^2dY$ corresponding to the elastic-elastic configuration at the two proton vertices

$$pp \longrightarrow \gamma\gamma \hookrightarrow e^+e^- \quad pp \qquad (64)$$

as well as the total two-photon contribution were integrated over Q_T^2 and Y. The resulting cross sections $d\sigma/dM^{(el.-el.,\ tot)}$ were then compared to the accurate, existing calculations in Ref. [3] for various values of s and M. The agreement turned out to be within ~ 5 %.

ii) After integration over Q_T^2 only, we have checked our two-photon cross section $d\sigma/dMdY/_{Y=0}$ against Ref. [5] for $s = 800\ GeV^2$ and $M^2/s = 0.2,\ 0.02$, and $\sqrt{s} = 800$ GeV, $M^2 = 120\ GeV^2$ and $M^2 = 7500\ GeV^2$ with good agreement.

iii) the <u>total</u> $\gamma\gamma$ contribution must clearly be symmetrical under the substitution $x_F \longleftrightarrow -x_F$. Hence the comparison of our numerical results at x_F and $-x_F$ provides a powerful test of the accuracy of the numerical method used. This test is particularly nontrivial, since with the integration variables used the integrand is not manifestly symmetrical in x_F.

† probably, because - for large Q_T - no variable transformation leading to an overall slowly varying integrand could be found.

On the one hand we faced the computation of a cross section depending on as many as four variables M, Q_T, x_F and $\sqrt{s}$. On the other hand we had to keep computer time within reasonable limits. Therefore we had to use rather large step sizes for our variables. In all our figures the points indicate the actually calculated values, whereas the curves are eyeball interpolations only.

3.2 The dominant configuration

The total $\gamma\gamma$ contribution is composed of a sum of terms corresponding to each of the two $p\gamma X$ vertices in Fig. 1 being either elastic or inelastic

$$d\sigma\,(pp \to \underset{\hookrightarrow \ell^+\ell^-}{\gamma\gamma}\, X) = d\sigma_{\text{el.-el.}} + d\sigma_{\text{el.-inel.}} + d\sigma_{\text{inel.-el.}} + d\sigma_{\text{inel.-inel.}} \quad (65)$$

In Figs. 3,4 we have displayed † the various contributions in Eq. (65) separately as functions of $\sqrt{s}$. Fig. 3 illustrates the situation for fixed (smallish) Q_T and fixed M, Fig. 4 refers to fixed $x_T = 2Q_T/\sqrt{s}$ and fixed $\tau = M^2/s$. At very small $Q_T \simeq 0.1$ GeV and fixed M the double elastic configuration clearly dominates up to very high $\sqrt{s}$, where the elastic-inelastic configuration takes over (Figs. 3a,b). At somewhat larger Q_T, the situation is quite different however (see Figs. 3c, d). There it is the elastic-inelastic configuration which is generally dominant, in particular over the presently accessible energy range. For fixed x_T and fixed τ the elastic-elastic contribution vanishes extremely fast with increasing $\sqrt{s}$. Ultimately, at very high energies, the double (deep) inelastic configuration takes over (Fig. 4).

The dominance of the el.-el. configuration for small Q_T and of the el.-inel. configuration for larger Q_T is an interesting result of our analysis. Its qualitative interpretation is: as long as Q_i^2 at a given vertex is kinematically allowed to remain small, this vertex prefers the elastic over the inelastic configuration with an almost on-shell photon. However, as soon as a Q_i^2 is forced by kinematics (large Q_T!) to become large at one vertex ($Q_i^2 \gtrsim m_\rho^2$), the suppression due to the elastic form factor is very much stronger than the

† for historical reasons the correction factor (41) has not been included in Figs. 3-5. This may affect somewhat the absolute values of cross sections for $Q_T \lesssim 1$ GeV.

one due to the (deep) inelastic structure function. Hence, in this case, the vertex becomes (deep) inelastic.

Our result has interesting experimental consequences: triggering on one elastic proton vertex does not reduce significantly the rate for $\gamma\gamma \to l^+l^-$ and $\gamma\gamma \to$ q-jet + $\bar{q}$-jet events and thus helps to identify these subprocesses.

Furthermore, working at large Q_T (and $\tau \neq 0$) automatically selects scattering of a highly virtual photon on an almost real photon target at the subprocess level:

i) the photon at the elastic vertex (Q_2, say) remains almost on shell ($Q_2^2 \lesssim m_\rho^2$) since the elastic proton (dipole) form factor strongly cuts off higher Q_2^2 in addition to the propagator effect $\propto 1/Q_2^4$.

ii) the second photon (Q_1) in turn, is pulled far off shell

$$Q_1^2 \gtrsim \sigma(Q_T^2) \to \infty \quad (66)$$

simply from kinematics (see appendix for $Q_{1,\min}^2$).

3.3 Results at fixed Q_T and M

This subsection contains our "realistic" results which are (or will be in due time) accessible to experiment.

Let us first point out the typical features of the two-photon Q_T distributions for fixed M. In Fig. 5 we display $d^3\sigma/dM^2 dQ_T^2 dY\,/_{Y=0}$ for $0.1 \leq Q_T \leq 7$ GeV at fixed M = 3 GeV and for four values of the energy from $\sqrt{s}$ = 27 to 800 GeV. A conspicuous feature is the very steep forward peak, coming mainly from the elastic-elastic proton vertex configuration (c.f. Figs. 3a,b). At values of $Q_T \gtrsim 2$ GeV the Q_T distribution flattens out considerably and becomes strongly energy dependent. Whereas at Q_T = 0.1 GeV the cross section increases only by a factor ~ 40 over the energy range considered, at Q_T = 7 GeV the increase amounts to four orders of magnitude. This effect becomes even more dramatic at higher masses M. Fig. 6 shows an increase by almost six orders of magnitude for M = 8.5 GeV and Q_T = 7 GeV.

Since we have four variables, Q_T, M, x_F and $\sqrt{s}$, at our disposal, we cannot possibly present results covering the whole kinematical range.

First generation experiments are obviously most likely to give results at smallish Q_T and M. Therefore, we present first of all in Tables 1 a-f the $\gamma\gamma$ contribution † to $pp \to \mu^+\mu^- X$ and $pp \to e^+e^- X$ at the ISR energy $\sqrt{s}$ = 63 GeV, for five values of Q_T ($0.05 \leq Q_T \leq 1.65$ GeV), three values of M (M = 4,6,8 GeV) and six values of $\hat{x}_F$ ($0 \leq \hat{x}_F \leq 0.8$). These values have been chosen such that integrations over any of the three variables, Q_T, M, and $\hat{x}_F$, can be performed with reasonable accuracy. In view of experiments at ISABELLE in the near future, we present a similar table, Table 2, at $\sqrt{s}$ = 800 GeV, with values of Q_T between 0.05 and 52 GeV, values of M ranging from 4 to 100 GeV and x_F = 0; the mass range has been chosen sufficiently large in view of experiments designed to measure in the mass region of the weak gauge boson. Notice also, that the two-photon contribution is equal for pp and $\bar{p}p$ collisions.

So far the presentation of our $\gamma\gamma$ results. Next, let us confront these results with existing ISR data at $\sqrt{s}$ = 63 GeV and with QCD estimates of the cross section at higher energies, in particular at $\sqrt{s}$ = 800 GeV.

First of all, we compare the calculated $\gamma\gamma$ contribution to recent two-photon candidate events [2] in $pp \to \mu^+\mu^- X$. To this end we integrate the theoretical $\gamma\gamma$ contribution at $\sqrt{s}$ = 62 GeV and x_F = 0.2 over M from 2.6 to 6.85 GeV and compare the resulting $d\sigma^{\gamma\gamma}/dQ_T dY\,/_{x_F=0.2}$ to the preliminary data †† of Ref. [2] in Fig. 7.

† Notice that for small values of Q_T the e^+e^- cross section is bigger than the $\mu^+\mu^-$ cross section (due to the electron-muon mass difference); the cross sections merge together around $Q_T \simeq 1.5$ GeV.

†† In Ref. [2] raw data for an unnormalized Q_T distribution - integrated over M from 2.6 to 6.85 GeV - at [22] x_F = 0.2 were presented. The Q_T acceptance is flat [22] for $Q_T \lesssim 1.8$ GeV. Using the absolute normalization given for $d\sigma^{\gamma\gamma}/dM$ in Ref. [2], the theoretical ratio $d\sigma^{\gamma\gamma}/dMdY\,|_{x_F=0.2} \Big/ d\sigma^{\gamma\gamma}/dM$ and the assumption that the selected events represent the full $\gamma\gamma$ contribution, we tentatively derived the absolute normalization of the Q_T histogram as shown in Fig. 7.

The qualitative agreement is quite encouraging, even though the data seem to be shifted by 200 - 300 MeV towards larger Q_T in comparison with the theoretical curve. One should, however, keep in mind that the experimental distribution may still have to be corrected [22] for effects of Q_T resolution, which may well result in an horizontal shift of the histogram. The separate theoretical contributions from the elastic-elastic and elastic-inelastic configurations of the $p\gamma X$ vertices are displayed as well in Fig. 7. Notice that the elastic-inelastic configuration dominates already at $Q_T \simeq 1$ GeV.

Next we come back to our qualitative argument in the introduction, which leads us to expect a considerable two-photon contribution at very small values of Q_T. Figs. 8 and 9 show that this is indeed the case and that the effect becomes increasingly important for increasing energy. In Fig. 8 ISR data [19] for $pp \to e^+e^- X$ - integrated over x_F and two mass intervals - are shown. With the help of Table 1 the corresponding theoretical $\gamma\gamma$ contributions are obtained. For $Q_T \simeq 0$ and smallish masses $4 \leq M \leq 4.5$ GeV the $\gamma\gamma$ contribution makes up as much as 70 % of the $pp \to e^+e^- X$ cross section. However, the $\gamma\gamma$ Q_T distribution is so steep, that its contribution, averaged over the first Q_T bin, $0 \leq Q_T \leq 0.5$ GeV, is down to 30 % and integrated over all Q_T down to a few percent. For somewhat higher masses, $\langle M \rangle \simeq 7$ GeV, the effect is less important ($\sim$ 25 % at $Q_T \simeq 0$).

Whereas at ISR energies the two-photon dominance is restricted to very small values of Q_T, at ISABELLE energies it is more dramatic and extends over the interval $0 \leq Q_T \lesssim 1$ GeV for masses $\gtrsim 10$ GeV. Fig. 9 shows the $\gamma\gamma$ cross section in comparison with an estimate of the QCD contribution to $pp \to l^+l^- X$. We used the $\mathcal{O}(\alpha_s)$QCD calculation, corrected for soft gluon radiation to all orders in leading bilogarithmic approximation of Ref. [8], normalized as described in Section 2.4; it is represented by the dashed curve. The encircled dots represent the $\mathcal{O}(\alpha_s)$ QCD calculation of Ref. [12]; obviously both QCD expressions overlap well down to intermediate values of Q_T (as necessary for internal consistency). We used the two mass values M^2 = 120 and 7500 GeV^2, for which the QCD calculations of Ref. [8] are available (M^2 = 7500 GeV^2, i.e. $M \simeq 87$ GeV, is in the expected Z-boson mass range). At this mass of 87 GeV the $\gamma\gamma$ dominance is dramatic (Fig. 9): at Q_T = 0.3 GeV the ratio $\gamma\gamma$/QCD for the e^+e^- ($\mu^+\mu^-$) final state is as much as $\sim$ 10 (6.4), averaged over a Q_T^2 - bin $0 \leq Q_T^2 \leq 1$ GeV^2 it is still 3.8 (2.4), whereas the ratio of the Q_T^2

integrated cross sections amounts to 0.25 (0.19) only. At the lower mass of M^2 = 120 GeV^2 ($\hat{=}$ M ≃ 11 GeV) the effect is less dramatic, but still significant (Fig. 9); for $Q_T \simeq 0.3$ GeV and an e^+e^- ($\mu^+\mu^-$) pair on finds $\gamma\gamma$/QCD ≃ 1 (0.7), if averaged from Q_T^2 = 0 to 1 GeV^2 $\langle \gamma\gamma \rangle / \langle$ QCD $\rangle \simeq$ 0.77 (0.46) and integrated over all Q_T^2 the ratio reduces to 0.24 (0.17). The Q_T^2 - integrated $\gamma\gamma$ cross sections are in good agreement with the results of Refs. [5] and [6]. Our analysis of the Q_T dependence has unravelled, however, that behind a sizeable, but not exciting ratio of the Q_T^2 - integrated $\gamma\gamma$ and QCD cross sections $\int dQ_T^2 (\gamma\gamma) / \int dQ_T^2$ QCD ≃ 0.2 there is hidden a ratio as large as 0.5 to 4 in the Q_T^2 bin $0 \leq Q_T^2 \leq 1$ GeV^2, depending on M and the l^+l^- final state.

It has been emphasized that an experimental signature for the resummed QCD contribution in leading bilogarithmic approximation is the flat shape [7,8,11] or even a turnover near $Q_T \simeq 0$ as well as the characteristic dependence [8,11] of the width of the forward peak on the mass M. Our results show that this effect is partly or fully swamped by the two-photon contribution.

Fig. 10 shows the mass dependence for fixed Q_T = 1.83 and 3.55 GeV and † $4 \leq M \leq 25$ GeV. This figure together with Figs. 12 and 14, which will be discussed in detail later, illustrate the situation for intermediate and large Q_T, $Q_T \gtrsim 1.5$ GeV say: at ISR energies and larger Q_T the $\gamma\gamma$ contribution is negligible everywhere (being of the order of a few percent), whereas at ISABELLE energies it amounts at least to 10 % almost everywhere and rises up to 20 % e.g. for Q_T = 1.83 GeV and $10 \lesssim M \lesssim 100$ GeV (see Figs. 9 and 10). It is still 14 % for Q_T = 3.55 GeV over a similar mass range.

3.4 Results at fixed x_T and τ

In this subsection we present our two-photon results in comparison with the $\mathcal{O}(\alpha_s)$ QCD contribution [12] to $pp \rightarrow l^+l^-X$ as functions of the variables $\hat{x}_T(x_T)$ and $\tau = M^2/s$ (remember $\hat{x}_T = x_T/(1-\tau) = Q_T/Q_{T\max}$). We do this more for completeness reasons, since smallness of the corresponding cross sections

† at $\sqrt{s}$ = 800 GeV the QCD calculation for $M \lesssim 10$ GeV is not trustworthy since for values $\sqrt{\tau} = M/\sqrt{s} \ll 0.02$ the involved consituent distributions (or-related to this - $d^2\sigma/dM\,dY/_{Y=0}$) are unknown.

will make measurements in most cases unlikely or impossible. Figs. 11 and 12 show the $\hat{x}_T$ (x_T) distributions for fixed values of τ and $\sqrt{s}$ at x_F = 0. For reasons of presentation all cross sections have been normalized to the two-photon cross-section at $\sqrt{s}$ = 27.3 GeV, which is displayed separately in Fig. 11 (at this energy $\mu^+\mu^-$ data exist for $\tau \lesssim 0.25$ and $\hat{x}_T \lesssim 0.34$).

The following global trend becomes evident from Fig. 12. If one keeps any two of the three variables τ, $\hat{x}_T$ and $\sqrt{s}$ fixed and increases the third one, the ratio $\gamma\gamma$/QCD increases. The $\gamma\gamma$ mechanism becomes important or even dominant if any two of the three variables become large; most dramatic is the effect for large values of τ (modulo uncertainties in the gluon distribution):

$$\begin{aligned} &\gamma\gamma/\text{QCD} \approx 100\ \%\ \text{e.g.} \\ &\text{at } \sqrt{s} = 63 \text{ GeV for} \begin{cases} (M \simeq 55 \text{ GeV},\ Q_T \simeq 2 \text{ GeV}) \\ M \simeq 40 \text{ GeV},\ Q_T \simeq 10 \text{ GeV} \end{cases} \\ &\text{at } \sqrt{s} = 800 \text{ GeV for} \begin{cases} (M \simeq 700 \text{ GeV},\ Q_T \simeq 10 \text{ GeV}) \\ M \simeq 400 \text{ GeV},\ Q_T \simeq 240 \text{ GeV} \end{cases} \end{aligned} \tag{67}$$

3.5 The x_F dependence

With the exception of Table 1 we have restricted our discussion so far to x_F = 0. Fig. 13 displays the $\hat{x}_F$ distribution of the $\gamma\gamma$ subprocess for a set of smallish values of τ and x_T and the two extreme energies $\sqrt{s}$ = 27 and 800 GeV. The weak energy dependence of the dimensionless quantity $sd^3\sigma / d\sqrt{\tau}\,dx_T^2 dY$ becomes evident from Fig. 13. Fig. 14 shows the $\gamma\gamma$ as well as the QCD contribution versus $\hat{x}_F$ for a set of large values of τ and x_T and all four energies. Table 1 contains in addition the $\hat{x}_F$ distribution of the $\gamma\gamma$ mechanism for various smallish values of Q_T and M at $\sqrt{s}$ = 63 GeV. From all these results we extract a simple, approximately factorizing behaviour (within a factor of two)

$$\frac{d^3\sigma}{dM^2\,dQ_T^2\,dY} \underset{\substack{\hat{x}_F \lesssim 0.5 \\ Q_T \neq 0}}{\approx} f(\hat{x}_F)\ F(M, Q_T, \sqrt{s}) \tag{68}$$

over the $\hat{x}_F$ range relevant for integrations over x_F. This may be useful for an estimate of the $\hat{x}_F$ integrated cross section in kinematical regions not discussed explicitely here.

4. Summary and Conclusions

We present the differential cross section for the two-photon mechanism $p^{(\bar{p})} \longrightarrow \gamma\gamma \hookrightarrow e^+e^- X$ in interesting kinematical regions of the four variables M, Q_T, x_F and $\sqrt{s}$ in form of tables and instructive figures. A comparison with $pp \longrightarrow l^+l^-X$ (including $pp \longrightarrow \gamma\gamma \hookrightarrow e^+e^- X$) data at ISR energies and with estimates of the QCD contribution to $pp \longrightarrow l^+l^-X$ elsewhere, in particular at very high energies, is performed.

We find important manifestations of the two-photon mechanism. Already at ISR energies and very small Q_T the $\gamma\gamma$ mechanism represents an important fraction (30 - 70 %, depending on M) of the $pp \longrightarrow e^+e^-X$ cross section; but it is negligible at larger Q_T. However, at ISABELLE energies, $\sqrt{s} \simeq 800$ GeV, its influence becomes dramatic: even if one averages over the fairly large Q_T^2 bin $0 \leq Q_T^2 \leq 1\ \text{GeV}^2$ one obtains for the ratio of $\gamma\gamma$ to QCD: $\langle \gamma\gamma \rangle / \langle \text{QCD} \rangle = 0.5 \div 4$, depending on M and the l^+l^- final state. Almost everywhere else the ratio still amounts to $\gamma\gamma/\text{QCD} \simeq 0.1 \div 0.2$. (For $M \approx \sqrt{s}$ the $\gamma\gamma$ mechanism becomes dominant again, however, the rates are tiny there).

Altogether, at ISABELLE, the $\gamma\gamma$ contribution becomes a serious background to the QCD contribution in particular for $Q_T \lesssim 2$ GeV. It totally swamps the experimental signature for the resummed QCD contribution in leading bi-logarithmic approximation, which predicts a flat shape if not a turnover near $Q_T \approx 0$, as well as a characteristic dependence of the flattening peak on M.

Let us, furthermore, point out that (at $\sqrt{s} = 800$ GeV) the $\gamma\gamma$ contribution also constitutes a sizeable fraction of the background in the search of the Z-boson in $pp \longrightarrow l^+l^-X$.

The two-photon mechanism is also an interesting process in its own right. This paper contains detailed information on the signature and on rates of two photon events in large parts of the kinematical range of the four variables M, Q_T, x_F and $\sqrt{s}$. There are two tables, for $\sqrt{s} = 63$ and 800 GeV which even allow integration over M or Q_T (or x_F).

The $\gamma\gamma$ mechanism is most easily accessible at small Q_T, where its rates are largest and where in addition it tends to dominate the $pp \to l^+l^-X$ cross section (absolute rates can be improved, of course by integrating over M and/or x_F).

A further clue for a future experimental isolation of the $\gamma\gamma$ mechanism comes from a decomposition into contributions from the two $p\gamma X$ vertices being both elastic, of mixed (elastic-inelastic) configuration or both inelastic. We find that for $Q_T \lesssim 1$ GeV the elastic-elastic contribution dominates, while for $Q_T \gtrsim 1$ GeV the elastic-inelastic one takes over. Thus triggering on one elastically scattered proton does not significantly reduce the $\gamma\gamma$ rate, whereas it may considerably reduce the background.

This may be particularly interesting for a possible isolation of the related subprocesses $\gamma\gamma \to$ q-jet + $\bar{q}$-jet and γ + gluon $\to$ q-jet + $\bar{q}$-jet, for which the present work is kind of a 'warming up' exercise. Insisting on an elastically scattered proton should - for colour and triality reasons - suppress the huge background from subprocesses like $q\bar{q} \to$ jets or gluon + q $\to$ jets. Left-over, 'higher-twist', subprocesses will decrease much faster with transverse momentum than the subprocesses of interest.

Finally, let us recall some uncertainties inherent in this investigation. As to our two-photon results, the only approximations made were the 'transverse photon' approximation (Sect. 2.2) and the parametrization used for the proton structure functions (Sect. 2.3), neglecting resonance fluctuations and scaling violations. As discussed, these approximations should not significantly affect our conclusions. As to the QCD reference cross section, scaling violations in the constituent distribution functions have been ignored as well. Moreover, we recall the uncertainties for very small values of $\tau \ll 0.02$ and also for large $\tau \to 1$. These limiting regimes of τ involve constituent distributions, where they are badly known.

Acknowledgements

We are very much indebted to P. Landshoff for inspiring discussions and active collaboration in the early stages of this work. We thank F. Vannucci and J. Field for valuable information about experimental aspects of two-photon physics.

We gratefully acknowledge the warm hospitality of the Department of Applied Mathematics and Theoretical Physics of Cambridge University and of the Physics Department of Durham University, where much of this work has been done.

One of us (F.S.) thanks the Science Research Council of Great Britain for a Senior Visiting Fellowship during his stay at Cambridge and Durham Universities.

Appendix

In this appendix we give the exact expressions for the integration limits in Eq. (28). Again, as in Sect. 3.1, numerical checks have been performed with the expressions below under $x_F \leftrightarrow -x_F$. Using

$$|\vec{q}_{iT}|^2 = \frac{Q_i^2}{x_i} u_i - \varepsilon \left(q_i^{02} + \frac{\bar{x}_T}{2} \frac{Q_i^2}{x_i} \cosh Y + \frac{Q_1^2 Q_2^2}{4m^2 x_1 x_2} \right) \quad (i=1,2) \tag{A1}$$

with

$$Q_i^2 = -q_i^2 \tag{A2}$$

$$\frac{2 q_{1,2}^0}{\sqrt{s}} = \bar{x}_T \cosh Y - \xi_{1,2} \mp \frac{1}{s} \left(\frac{Q_1^2}{x_1} - \frac{Q_2^2}{x_2} \right) \tag{A3}$$

$$\xi_{1,2} = \frac{\bar{x}_T}{2} \left(\cosh Y \mp \sqrt{\frac{s-4m^2}{s}} \sinh Y \right) \tag{A4}$$

$$u_{1,2} = x_{1,2} - \frac{1}{2} \bar{x}_T \left(\cosh Y \pm \sqrt{\frac{s}{s-4m^2}} \sinh Y \right) \tag{A5}$$

$$\varepsilon = \frac{4m^2}{s-4m^2} \quad ; \quad \bar{x}_T = \sqrt{4\tau + x_T^2} \tag{A6}$$

one may express the "triangle" function $\sqrt{-\lambda}$ in the Jacobian (20) - after a straight forward but tedious calculation as

$$\sqrt{-\lambda(Q_T^2, |\vec{q}_{1T}|^2, |\vec{q}_{2T}|^2)} = \sqrt{\left\{ \left(\frac{u_2}{x_2} \right)^2 + \varepsilon \left(\frac{x_T}{2x_2} \right)^2 \right\} (Q_2^2 - Q_{2,\min}^2)(Q_{2,\max}^2 - Q_2^2)} \tag{A7}$$

with limits of the Q_2^2 integration determined as

$$Q_{2\ \min}^{2\ \max} = \frac{x_2}{2a} \left(-b \pm \sqrt{b^2 - 4ac} \right) \tag{A8}$$

where

$$a = u_2^2 + \varepsilon \frac{x_T^2}{4} \tag{A9}$$

$$b = 2 \left[-\frac{Q_1^2}{x_1} u_1 u_2 + \frac{x_T^2}{4} \left((2+\varepsilon) \frac{Q_1^2}{x_1} - s u_2 + \varepsilon s \xi_2 \right) + \frac{\varepsilon}{4} s \left(\xi_2^2 - \xi_1^2 \right) u_2 \right] \tag{A10}$$

$$c = \left(s \left(\frac{x_T}{2} \right)^2 - \frac{u_1 Q_1^2}{x_1} \right)^2 + \frac{\varepsilon \cdot s}{2} \left[\frac{x_T^2 Q_1^2}{x_1} \xi_1 + s \left(\frac{x_T}{2} \right)^2 (\xi_1^2 + \xi_2^2) - \frac{u_1 Q_1^2}{x_1} (\xi_2^2 - \xi_1^2) \right] + \left(\frac{\varepsilon s}{4} (\xi_2^2 - \xi_1^2) \right)^2 + \varepsilon \left(\frac{x_T Q_1^2}{2 x_1} \right)^2 \tag{A11}$$

The equation $b^2 - 4ac = 0$, being quadratic in Q_1^2, leads to the following limits of the Q_1^2 integration

$$Q_{1\ \min}^{2\ \max} = \frac{x_1}{2A} \left(-B \mp \sqrt{B^2 - 4AC} \right) \tag{A12}$$

with

$$A = 4 \left(\left(\frac{x_T}{2} \right)^2 - u_1 u_2 \right) + \varepsilon \left(x_T^2 - (u_1 + u_2)^2 \right) \tag{A13}$$

$$B = s \left[4 u_2 \left(u_1 u_2 - \left(\frac{x_T}{2} \right)^2 \right) - 2 \varepsilon \xi_2 u_1 u_2 + \varepsilon \frac{x_T^2}{2} (u_1 - u_2 + 2\xi_2) - 2 \varepsilon \xi_1 u_2^2 + \varepsilon (\xi_2^2 - \xi_1^2) \left(u_2 + \frac{\varepsilon}{2} (u_1 + u_2) \right) + \varepsilon^2 \frac{x_T^2}{2} (\xi_2 - \xi_1) \right] \tag{A14}$$

$$C = \varepsilon \cdot s^2 \left[-\left(\left(\frac{x_T}{2} \right)^2 + \xi_2 u_2 \right)^2 + \frac{\varepsilon}{2} (\xi_2^2 - \xi_1^2) \cdot \left(\left(\frac{x_T}{2} \right)^2 + \xi_2 u_2 - \frac{\varepsilon}{8} (\xi_2^2 - \xi_1^2) \right) \right]. \tag{A15}$$

Let $u_1^{(\pm)}$ be the roots of the equation $B^2 - 4AC = 0$, quadratic in u_1:

$$u_1^{(\pm)} = \frac{1}{2\alpha} \left(-\beta \pm \sqrt{\beta^2 - 4\alpha\gamma} \right) \tag{A16}$$

and

$$\alpha = u_2^4 + \varepsilon u_2^2\left(\left(\frac{x_T}{2}\right)^2 - \xi_2 u_2\right) + \varepsilon^2\left(\frac{u_2^2}{4}\left(\xi_2^2-\xi_1^2\right) - \left(\frac{x_T}{2}\right)^2 \xi_2 u_2\right) + \frac{\varepsilon^3}{4}\left(\frac{x_T}{2}\right)^2\left(\xi_2^2-\xi_1^2\right) \tag{A17}$$

$$\begin{aligned}\beta = {} & u_2^3\left[-\frac{x_T^2}{2} + \varepsilon\left(-\xi_1 u_2 - \left(\frac{x_T}{2}\right)^2 - \frac{1}{2}\left(\xi_1^2+\xi_2^2\right)\right)\right] \\ & + \varepsilon\left(\left(\frac{x_T}{2}\right)^2 \xi_2 u_2^2 - 2\left(\frac{x_T}{2}\right)^4 u_2\right) + \varepsilon^2\left[-\frac{u_2^3}{4}\left(\xi_2-\xi_1\right)^2 + \right. \\ & \frac{u_2^2}{4}\xi_2\left(\xi_2^2-\xi_1^2\right) + \frac{x_T^2}{8}\left(\xi_2 - 3\xi_1\right)u_2^2 - \left(\frac{x_T}{2}\right)^2\frac{1}{2}\left(\xi_1^2+\xi_2^2\right)u_2 \\ & \left. - \left(\frac{x_T}{2}\right)^4\left(u_2-\xi_2\right)\right] + \varepsilon^3\left[u_2^2\frac{1}{8}\left(\xi_2^2-\xi_1^2\right)\left(\xi_2-\xi_1\right) - u_2\left(\frac{x_T}{2}\right)^2 \cdot\right. \\ & \cdot\frac{1}{4}\left(\xi_2-\xi_1\right)^2 + \left(\frac{x_T}{2}\right)^4\frac{1}{2}\left(\xi_2-\xi_1\right) + \left(\frac{x_T}{2}\right)^2\xi_2\frac{1}{4}\left(\xi_2^2-\xi_1^2\right)\Big] \\ & + \varepsilon^4\left(\frac{x_T}{2}\right)^2\frac{1}{8}\left(\xi_2-\xi_1\right)^2\left(\xi_1+\xi_2\right)\end{aligned} \tag{A18}$$

$$\begin{aligned}\gamma = {} & \left(u_2\left(\frac{x_T}{2}\right)^2\right)^2 + \varepsilon\left(\frac{x_T}{2}\right)^2\left[\xi_1 u_2^3 + \left(\frac{x_T}{2}\right)^2 u_2^2 + u_2^2\frac{1}{2}\left(\xi_1^2+\xi_2^2\right)\right. \\ & \left. + \left(\frac{x_T}{2}\right)^4\right] + \varepsilon^2\left[-u_2^3\frac{1}{4}\left(\xi_2^2-\xi_1^2\right)\left(u_2+\xi_1\right) + u_2^2\frac{1}{2}\left(\xi_2-\xi_1\right)\cdot\right. \\ & \cdot\left\{-u_2\left(\frac{x_T}{2}\right)^2 + \frac{1}{8}\left(\xi_1+\xi_2\right)^2\left(\xi_2-\xi_1\right) + \left(\frac{x_T}{2}\right)^2\left(\xi_2-\xi_1\right)\right\} \\ & \left. + \left(\frac{x_T}{2}\right)^4\left(\xi_1 u_2 + \frac{1}{2}\left(\xi_1^2+\xi_2^2\right) + \left(\frac{x_T}{2}\right)^2\right)\right] + \varepsilon^3\left[\frac{1}{4}\left(\xi_2^2-\xi_1^2\right)\right. \\ & \cdot\left\{\frac{1}{2}\left(\xi_2-\xi_1\right)u_2^3 + u_2^2\frac{1}{4}\left(\xi_2^2-\xi_1^2\right) - \left(\frac{x_T}{2}\right)^2\xi_1 u_2 + \right. \\ & \left.\left. + \left(\frac{x_T}{2}\right)^2\frac{1}{4}\left(\xi_2^2-\xi_1^2\right)\right\} - \frac{1}{2}\left(\xi_2-\xi_1\right)\left\{\xi_1 u_2^2\left(\frac{x_T}{2}\right)^2\right. \right. \\ & \left.\left. + u_2\left(\frac{x_T}{2}\right)^4 - \left(\frac{x_T}{2}\right)^4\left(\xi_2-\xi_1\right)\right\}\Big] + \varepsilon^4\frac{1}{4}\left(\xi_2^2-\xi_1^2\right)\left(\frac{x_T}{2}\right)^2\cdot \\ & \cdot\left[u_2\frac{1}{2}\left(\xi_2-\xi_1\right) + \left(\frac{x_T}{2}\right)^2\frac{\xi_2-\xi_1}{\xi_2+\xi_1} + \frac{1}{4}\left(\xi_2^2-\xi_1^2\right)\right]\end{aligned} \tag{A19}$$

then the limits of the x_1 integration, depending on x_2, are given by (using Eq. (A5))

$$x_{1,\min} = \max\left(u_1^{(+)}, u_1^{(-)}\right) + \frac{\bar{x}_T}{2}\left(\cosh\gamma + \sqrt{\frac{s}{s-4m^2}}\sinh\gamma\right) \tag{A20}$$

$$x_{1,\max} = 1$$

In the limit $\varepsilon \to 0$, the complicated expressions (A16 - A20) reduce simply to

$$x_{1,\min} - \frac{\bar{x}_T}{2}e^{\gamma} = u_1^{(+)} = u_1^{(-)} = \left(\frac{x_T}{2}\right)^2 \Big/ u_2 = \left(\frac{x_T}{2}\right)^2 \Big/ \left(x_2 - \frac{\bar{x}_T}{2}e^{-\gamma}\right) \tag{A21}$$

Finally, the limits of the x_2 integration are obtained by the substitution

$$x_{2,\min} = x_{1,\min}\left(\xi_2 \leftrightarrow \xi_1,\ u_2 \to u_1(x_1=1)\right)$$

in Eqs. (A20, A21) and

$$x_{2,\max} = 1. \tag{A22}$$

Table 1 : Two-photon cross sections $d^3\sigma/dMdQ_T^2dY$ in nb/GeV^3 for $p\bar{p} \to \gamma\gamma X \to \mu^+\mu^- X$ and $p\bar{p} \to \gamma\gamma X \to e^+e^- X$ versus M [GeV], Q_T [GeV] and $\hat{x}_F$ at $\sqrt{s}$ = 63 GeV. The numbers in parentheses refer to e pairs the others to μ pairs.

Q_T \ M	2	4	6	8
0.05	$4.6\ 10^{-1}$ ($1.0\ 10^{0}$)	$2.0\ 10^{-2}$ ($3.5\ 10^{-2}$)	$2.8\ 10^{-3}$ ($4.5\ 10^{-3}$)	$6.2\ 10^{-4}$ ($9.4\ 10^{-4}$)
0.45	$3.8\ 10^{-2}$ ($5.1\ 10^{-2}$)	$4.4\ 10^{-3}$ ($5.9\ 10^{-3}$)	$9.4\ 10^{-4}$ ($1.3\ 10^{-3}$)	$2.7\ 10^{-4}$ ($3.7\ 10^{-4}$)
0.85	$6.8\ 10^{-3}$ ($7.7\ 10^{-3}$)	$1.0\ 10^{-3}$ ($1.2\ 10^{-3}$)	$2.4\ 10^{-4}$ ($2.8\ 10^{-4}$)	$7.7\ 10^{-5}$ ($9.0\ 10^{-5}$)
1.25	$1.4\ 10^{-3}$ ($1.5\ 10^{-3}$)	$3.0\ 10^{-4}$ ($3.2\ 10^{-4}$)	$8.0\ 10^{-5}$ ($8.6\ 10^{-5}$)	$2.6\ 10^{-5}$ ($2.8\ 10^{-5}$)
1.65	$4.0\ 10^{-4}$ ($3.9\ 10^{-4}$)	$1.1\ 10^{-4}$ ($1.1\ 10^{-4}$)	$3.2\ 10^{-5}$ ($3.3\ 10^{-5}$)	$1.1\ 10^{-5}$ ($1.1\ 10^{-5}$)

a) $\hat{x}_F = 0$

Q_T \ M	4	6	8
0.05	$1.2\ 10^{-2}$ ($2.1\ 10^{-2}$)	$2.1\ 10^{-3}$ ($3.4\ 10^{-3}$)	$5.5\ 10^{-4}$ ($8.3\ 10^{-4}$)
0.45	$3.7\ 10^{-3}$ ($5.2\ 10^{-3}$)	$8.3\ 10^{-4}$ ($1.1\ 10^{-3}$)	$2.5\ 10^{-4}$ ($3.4\ 10^{-4}$)
0.85	$8.1\ 10^{-4}$ ($9.4\ 10^{-4}$)	$2.1\ 10^{-4}$ ($2.4\ 10^{-4}$)	$6.8\ 10^{-5}$ ($8.0\ 10^{-5}$)
1.25	$2.4\ 10^{-4}$ ($2.5\ 10^{-4}$)	$6.8\ 10^{-5}$ ($7.3\ 10^{-5}$)	$2.3\ 10^{-5}$ ($2.5\ 10^{-5}$)
1.65	$8.4\ 10^{-5}$ ($8.6\ 10^{-5}$)	$2.7\ 10^{-5}$ ($2.8\ 10^{-5}$)	$9.8\ 10^{-6}$ ($1.0\ 10^{-5}$)

b) $\hat{x}_F = 0.1$

Table 1 (cont.)

Q_T \ M	4	6	8
0.05	$7.1\ 10^{-3}$ ($1.2\ 10^{-2}$)	$1.4\ 10^{-3}$ ($2.2\ 10^{-3}$)	$4.2\ 10^{-4}$ ($6.2\ 10^{-4}$)
0.45	$2.7\ 10^{-3}$ ($3.9\ 10^{-3}$)	$6.1\ 10^{-4}$ ($8.4\ 10^{-4}$)	$1.9\ 10^{-4}$ ($2.6\ 10^{-4}$)
0.85	$5.4\ 10^{-4}$ ($6.4\ 10^{-4}$)	$1.5\ 10^{-4}$ ($1.8\ 10^{-4}$)	$5.2\ 10^{-5}$ ($6.1\ 10^{-5}$)
1.25	$1.4\ 10^{-4}$ ($1.5\ 10^{-4}$)	$4.6\ 10^{-5}$ ($5.0\ 10^{-5}$)	$1.7\ 10^{-5}$ ($1.8\ 10^{-5}$)
1.65	$5.0\ 10^{-5}$ ($5.0\ 10^{-5}$)	$1.8\ 10^{-5}$ ($1.9\ 10^{-5}$)	$7.0\ 10^{-6}$ ($7.2\ 10^{-6}$)

c) $\hat{x}_F = 0.2$

Q_T \ M	4	6	8
0.05	$4.5\ 10^{-3}$ ($7.6\ 10^{-3}$)	$9.2\ 10^{-4}$ ($1.4\ 10^{-3}$)	$2.9\ 10^{-4}$ ($4.2\ 10^{-4}$)
0.45	$1.7\ 10^{-3}$ ($2.5\ 10^{-3}$)	$3.9\ 10^{-4}$ ($5.3\ 10^{-4}$)	$1.3\ 10^{-4}$ ($1.7\ 10^{-4}$)
0.85	$3.1\ 10^{-4}$ ($3.7\ 10^{-4}$)	$9.2\ 10^{-5}$ ($1.1\ 10^{-4}$)	$3.3\ 10^{-5}$ ($3.9\ 10^{-5}$)
1.25	$7.6\ 10^{-5}$ ($8.2\ 10^{-5}$)	$2.7\ 10^{-5}$ ($2.8\ 10^{-5}$)	$1.0\ 10^{-5}$ ($1.1\ 10^{-5}$)
1.65	$2.5\ 10^{-5}$ ($2.5\ 10^{-5}$)	$1.0\ 10^{-5}$ ($1.0\ 10^{-5}$)	$4.2\ 10^{-6}$ ($4.3\ 10^{-6}$)

d) $\hat{x}_F = 0.3$

Q_T \ M	4	6	8
0.05	$1.2\ 10^{-3}$	$2.6\ 10^{-4}$	$8.0\ 10^{-5}$
0.45	$3.7\ 10^{-4}$	$9.6\ 10^{-5}$	$3.3\ 10^{-5}$
0.85	$5.9\ 10^{-5}$	$2.0\ 10^{-5}$	$7.9\ 10^{-6}$
1.25	$1.3\ 10^{-5}$	$5.2\ 10^{-6}$	$2.3\ 10^{-6}$
1.65	$3.9\ 10^{-6}$	$1.9\ 10^{-6}$	$8.9\ 10^{-7}$

e) $\hat{x}_F = 0.5$

Q_T \ M	4	6	8
0.05	$8.1\ 10^{-6}$	$2.5\ 10^{-6}$	$9.4\ 10^{-7}$
0.45	$2.6\ 10^{-6}$	$9.3\ 10^{-7}$	$3.9\ 10^{-7}$
0.85	$3.5\ 10^{-7}$	$1.7\ 10^{-7}$	$8.2\ 10^{-8}$
1.25	$6.4\ 10^{-8}$	$3.7\ 10^{-8}$	$2.1\ 10^{-8}$
1.65	$1.7\ 10^{-8}$	$1.1\ 10^{-8}$	$6.8\ 10^{-9}$

f) $\hat{x}_F = 0.8$

Table 2 : Same as Table 1 for $\sqrt{s}$ = 800 GeV and $x_F = 0$

Q_T \ M	4	10.95	52	86.64	100
0.05	$1.4\ 10^{-2}$ ($2.3\ 10^{-2}$)	$8.6\ 10^{-4}$ ($1.4\ 10^{-3}$)	$7.5\ 10^{-6}$ ($1.2\ 10^{-5}$)	$1.2\ 10^{-6}$ ($2.0\ 10^{-6}$)	$6.9\ 10^{-7}$ ($1.1\ 10^{-6}$)
0.45	$1.5\ 10^{-2}$ ($2.3\ 10^{-2}$)	$8.9\ 10^{-4}$ ($1.4\ 10^{-3}$)	$5.6\ 10^{-6}$ ($9.1\ 10^{-6}$)	$7.2\ 10^{-7}$ ($1.2\ 10^{-6}$)	$3.8\ 10^{-7}$ ($6.1\ 10^{-7}$)
0.85	$4.1\ 10^{-3}$ ($5.4\ 10^{-3}$)	$2.5\ 10^{-4}$ ($3.5\ 10^{-4}$)	$1.3\ 10^{-6}$ ($2.0\ 10^{-6}$)	$1.7\ 10^{-7}$ ($2.4\ 10^{-7}$)	$8.6\ 10^{-8}$ ($1.3\ 10^{-7}$)
1.65	$7.6\ 10^{-4}$ ($8.6\ 10^{-4}$)	$6.8\ 10^{-5}$ ($8.3\ 10^{-5}$)	$3.5\ 10^{-7}$ ($4.5\ 10^{-7}$)	$3.9\ 10^{-8}$ ($5.1\ 10^{-8}$)	$2.0\ 10^{-8}$ ($2.6\ 10^{-8}$)
4	$2.7\ 10^{-5}$	$6.9\ 10^{-6}$ ($7.6\ 10^{-6}$)	$5.6\ 10^{-8}$ ($6.5\ 10^{-8}$)	$6.4\ 10^{-9}$ ($7.4\ 10^{-9}$)	$3.3\ 10^{-9}$ ($3.8\ 10^{-9}$)
20	$\approx 6.3\ 10^{-9}$	$7.7\ 10^{-9}$	$8.1\ 10^{-10}$	$1.4\ 10^{-10}$	$8.3\ 10^{-11}$
36	$\approx 1.2\ 10^{-10}$	$2.3\ 10^{-10}$	$6.5\ 10^{-11}$	$1.7\ 10^{-11}$	$1.1\ 10^{-11}$
52	$\approx 7.6\ 10^{-12}$	$1.7\ 10^{-11}$	$1.0\ 10^{-11}$	$3.2\ 10^{-12}$	$2.1\ 10^{-12}$

Figure Captions

Figure 1: Kinematics of the process $pp \to \gamma\gamma X$, $\gamma \to \ell^+\ell^-$.

Figure 2: The optical theorem for $pp \to \gamma\gamma X$, $\gamma \to \ell^+\ell^-$.

Figure 3: The (transverse) $\gamma\gamma$ contribution to $p^{(-)}p \to \mu^+\mu^- X$ for different smallish values of Q_T and M as a function of $\sqrt{s}$. The total contribution (——●——) as well as its decomposition into the three different components corresponding to both proton vertices being elastic (——▲——); inelastic (— —o— —) and to the sum of the mixed configurations (— —×— —) are displayed.

Figure 4: The (transverse) $\gamma\gamma$ contribution to $p^{(-)}p \to \mu^+\mu^- X$ at fixed small $\hat{x}_T = x_T/(1-\tau) = 0.04$ and two values of τ as a function of $\sqrt{s}$. The decomposition is as in Fig. 3.

Figure 5: The Q_T distribution of the (transverse) $\gamma\gamma$ contribution to $p^{(-)}p \to \mu^+\mu^- X$ for M = 3 GeV and four energies ($27.3 \leq \sqrt{s} \leq 800$ GeV) at small and intermediate values of Q_T.

Figure 6: The quantity $Q_T^4\, d^3\sigma/dM^2 dQ_T^2 dY|_{Y=0}$ ($p^{(-)}p \to (\gamma\gamma)_T X$, $\gamma \to \mu^+\mu^-$) versus Q_T for M = 3 and 8.5 GeV and four energies ($27.3 \leq \sqrt{s} \leq 800$ GeV). This Figure illustrates the dramatic energy dependence at larger Q_T.

Figure 7: The histogram shows the Q_T distribution of $\gamma\gamma$ candidate events [2] in $pp \to \mu^+\mu^- X$ as measured at the ISR for $\sqrt{s}$ = 62 GeV and x_F = 0.2. The distribution is integrated over the mass interval $2.6 \leq M \leq 6.85$ GeV. The tentative absolute normalization was obtained by us in Section 3.3. For comparison the theoretical prediction for the (transverse) $\gamma\gamma$ contribution is displayed (————) as well as its decomposition into contributions from both proton vertices being elastic (—·—·) and from one being elastic and the other one inelastic (— — —).

Figure 8: ISR data [19] for the cross section $d\sigma/dQ_T^2$ ($pp \to e^+e^-X$), integrated over x_F and two different mass intervals are displayed. The solid lines denote our calculated two-photon contributions to this process.

Figure 9: Q_T distributions for $pp \to l^+l^-X$ at $\sqrt{s}$ = 800 GeV and $x_F = 0$ for the two mass values used in Ref.[8], M^2 = 120 GeV^2 ($\hat{=}$ M $\approx$ 11 GeV) and M^2 = 7500 GeV^2 ($\hat{=}$ M $\simeq$ 87 GeV). The solid lines (——●——) and (——○——) denote the $\gamma\gamma$ contributions to $pp \to e^+e^-X$ and $pp \to \mu^+\mu^-X$ respectively and (— — — — —) denotes the resummed QCD contribution to $pp \to l^+l^-X$ including soft gluon emission to all orders in leading bilogarithmic approximation. It was given in Ref.[8] in unnormalized form for $Q_T \gtrsim 0.3$ GeV and normalized by us in Sect. 2.4 to the $\mathcal{O}(\alpha_s)$ expression of Ref.[12] (encircled dots) at larger Q_T.

Figure 10a): The quantity $M^4 d^3\sigma/dM^2dQ_T^2dY|_{Y=0}(pp \to \mu^+\mu^-X)$ versus M for two intermediate values of Q_T and four energies ($27.3 \leq \sqrt{s} \leq 800$ GeV). The solid line denotes the (transverse) $\gamma\gamma$ contribution, the dash-dotted one the $\mathcal{O}(\alpha_s)$ QCD contribution of Ref.[12].

10b): The ratio $(\gamma\gamma)_T/QCD$ of the quantities in a).

Figure 11: The $\hat{x}_T$ (= $x_T/(1-\tau)$) distribution of the (transverse) $\gamma\gamma$ contribution to $p\bar{p} \to \mu^+\mu^-X$ for four fixed values of τ ($0.09 \leq \tau \leq 0.81$) and the lowest energy considered, $\sqrt{s}$ = 27.3 GeV.

Figure 12: The $\hat{x}_T$ (x_T) distribution of the (transverse) $\gamma\gamma$ contribution (——————) to $pp \to \mu^+\mu^-X$ in comparison to the $\mathcal{O}(\alpha_s)$ QCD contribution of Ref.[12] (— · — · —) for four fixed values of τ ($0.09 \leq \tau \leq 0.81$) and four energies ($27.3 \leq \sqrt{s} \leq 800$ GeV). All $\hat{x}_T$ (x_T) distributions are normalized by the $\gamma\gamma$ distribution for $\sqrt{s}$ = 27.3 GeV (Fig. 11). The lower abszissa refers to the variable $\hat{x}_T = Q_T/Q_{T,max} \simeq x_T/(1-\tau)$ (with $0 \leq \hat{x}_T \leq 1$) and the upper one to $x_T = 2Q_T/\sqrt{s}$.

Figure 13: The distribution of the (transverse) $\gamma\gamma$ contribution to $p(\bar{p}) \to \mu^+\mu^-X$ in the Feynman type variable $\hat{x}_F = Q_L/Q_{L,max}$ for small values of τ = 0.063 and x_T = 0.04 and for the lowest and highest energies considered: $\sqrt{s}$ = 27.3 and 800 GeV.

Figure 14: The distribution of the (transverse) $\gamma\gamma$ contribution to $pp \to \mu^+\mu^-X$, (——————), in the Feynman type variable $\hat{x}_F = Q_L/Q_{L,max}$ in comparison to the $\mathcal{O}(\alpha_s)$ QCD contribution of Ref.[12], (— · — · —), for largish values of τ = 0.25 and x_T = 0.52 and four different energies ($27.3 \leq \sqrt{s} \leq 800$ GeV).

References

1. Ch. Berger, Talk at the Int. Workshop on $\gamma\gamma$ Collisions, Amiens, April 8-12, 1980, RWTH-Aachen report PITHA 80/07 (1980);
   W. Wagner, Talk at the 20th Int. Conf. on High Energy Physics, Madison, Wisc., July 17-23, 1980.

2. CERN-Harvard-LAPP-MIT-Naples-Pisa Collaboration:
   F. Vannucci, Talk at the Int. Workshop on $\gamma\gamma$ Collisions, Amiens, April 8-12, 1980, CERN-EP/80-82 (1980).

3. M.-S. Chen, I.J. Muzinich, H. Terazawa and T.P. Cheng, Phys. Rev. D7, 3485 (1973).

4. V.M. Budnev, I.F. Ginzburg, G.V. Meledin and V.G. Serbo, Sov. J. Particles Nucl. 4, 100 (1973); Phys. Rep. 15C, 181 (1975).

5. C. Carimalo, P. Kessler and J. Parisi, Phys. Rev. D18, 2443 (1978).

6. R. Moore, Z. Physik C, Particles and Fields 5, 351 (1980).

7. Yu.L. Dokshitzer, D.I. Dyakonov and S.I. Troyan, Phys. Lett. 78B, 290 (1978); 79B, 269 (1978); Phys. Rep. 58, 269 (1980).

8. G. Parisi and R. Petronzio, Nucl. Phys. B154, 427 (1979).

9. C. L. Basham, L.S. Brown, S.D. Ellis and S.T. Love, Phys. Lett. 85B, 297 (1979)

10. C.Y.Lo and J.D. Sullivan, Phys. Lett. 86B, 327 (1979)

11. S.D. Ellis and W.J. Stirling, Univ. Washington, Seattle, Preprint, RLO-1388-821 (1980).

12. K. Kajantie and R. Raitio, Nucl. Phys. B139, 72 (1978).

13. G. Altarelli, G. Parisi and R. Petronzio, Phys. Lett. 76B, 356 (1978).

14. E.D. Bloom and F.J. Gilman, Phys. Rev. D4, 2901 (1971).

15. G. Fox, Nucl. Phys. B131, 107 (1977).

16. B. Schrempp and F. Schrempp, Z. Physik C, Particles and Fields 6, 7 (1980).

17. J.K.Yoh et al., Phys. Rev. Lett. 41, 684 (1978).

18. CERN-Harvard-MIT-Naples-Pisa Collaboration:
   U. Becker, Proc. Int. Conf. on High Energy Physics, Geneva, June 27 - July 4, 1979, Vol. 2, p. 779.

19. Athens-BNL-CERN-Syracuse-Yale Collaboration:
   C. Kourkoumelis et al., Phys. Lett. 91B, 475 (1980).

20. CERN-Columbia-Oxford-Rockefeller Collaboration:
   A.L.S. Angelis et al., Proc. Int. Conf. on High Energy Physics, Geneva, June 27 - July 4, 1979, Vol. 2, p. 770.

21. A.J. Clark et al., Nucl. Phys. B142, 29 (1978).

22. F. Vannucci, private communication.

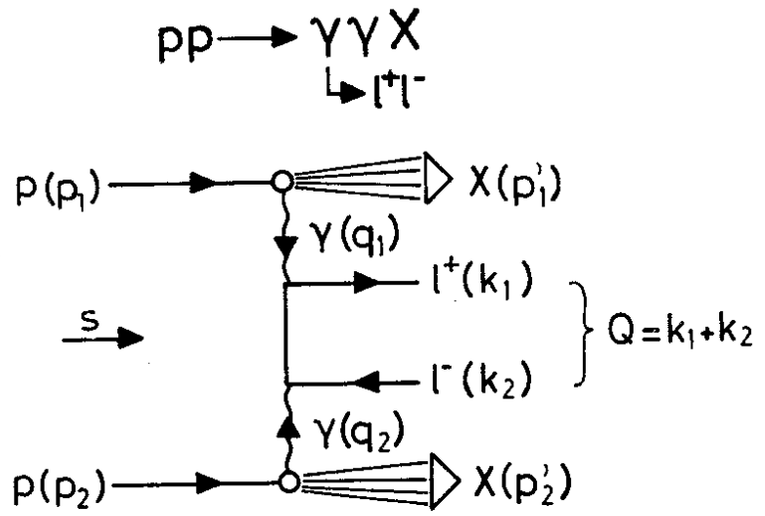

$M^2 \equiv Q^2$

$\vec{Q}_T = (\vec{k}_1 + \vec{k}_2)_T = (\vec{q}_1 + \vec{q}_2)_T$

$x_F = \frac{2Q_L}{\sqrt{s}}$

$x_i = \frac{-q_i^2}{2p_i \cdot q_i} \quad (i=1,2)$

$Q_i^2 = -q_i^2 > 0$

Fig.1

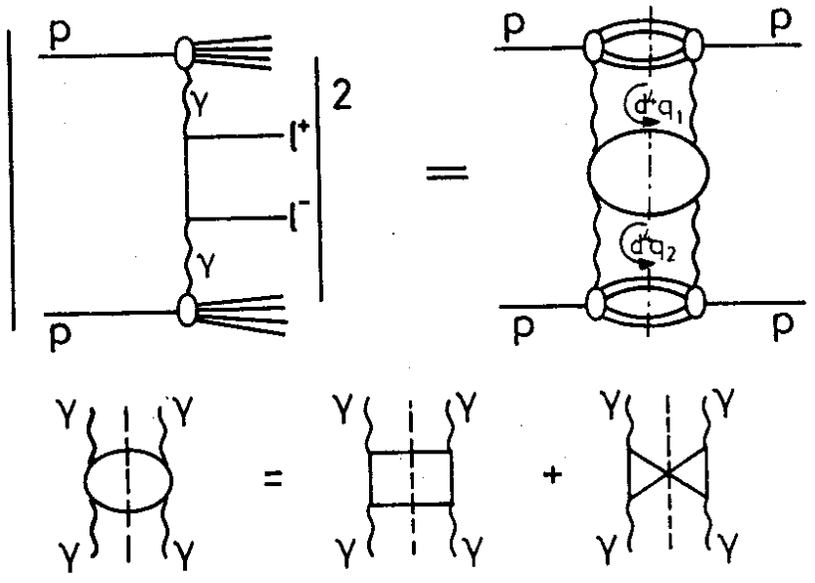

Fig. 2

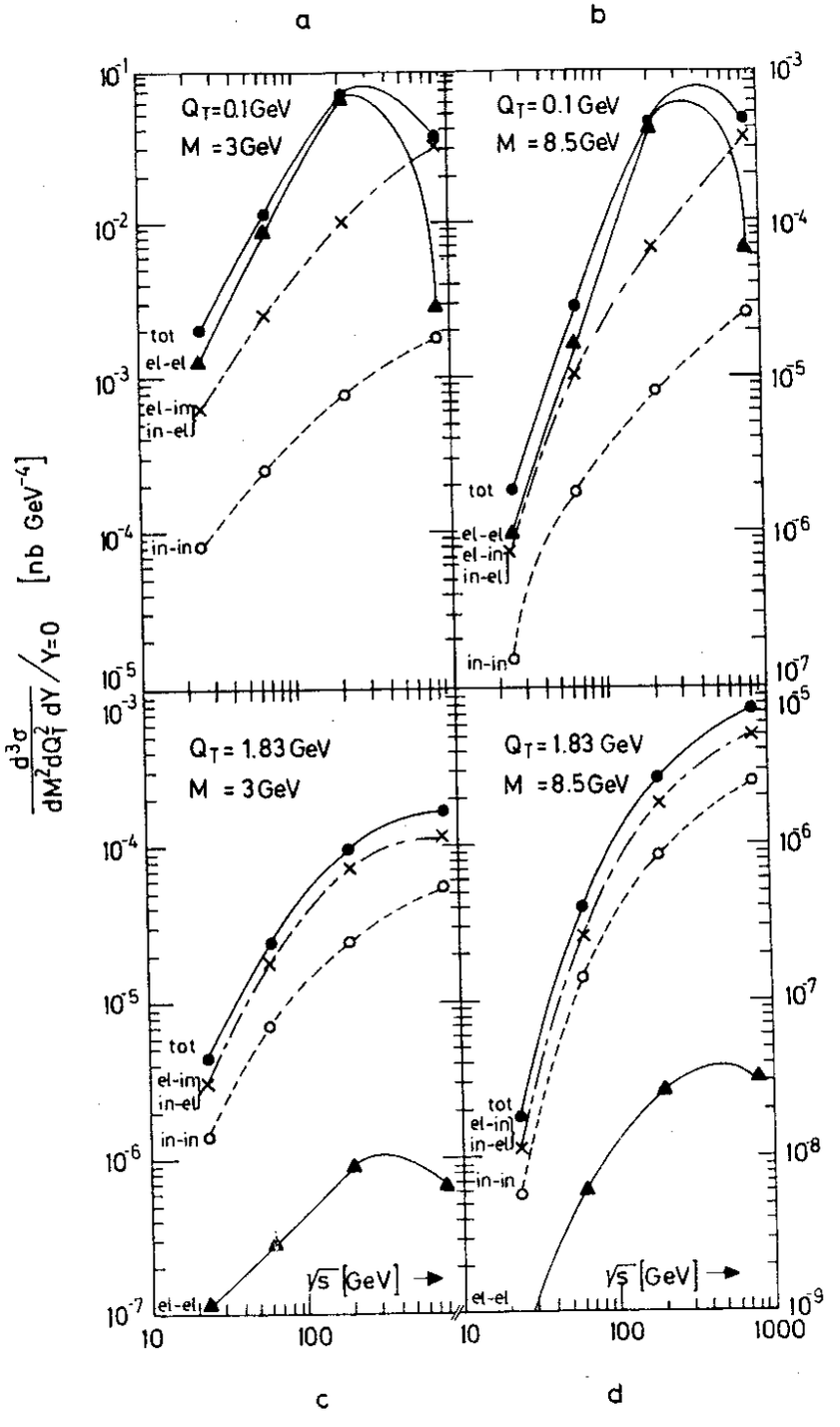

Fig.3

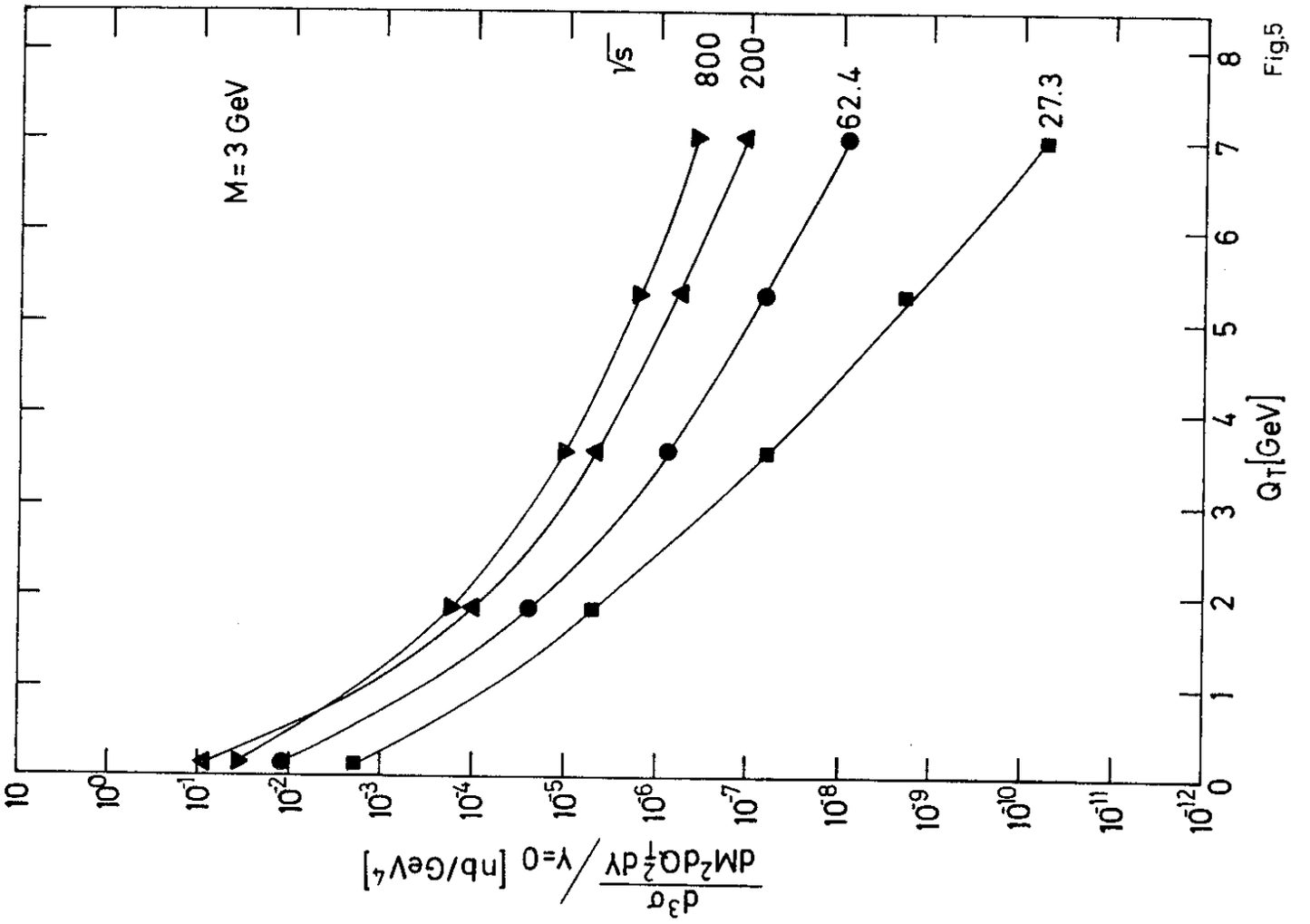
M = 3 GeV
√s
800
200
62.4
27.3
$\frac{d^3\sigma}{dM^2 dQ_T^2 dY}\Big/_{Y=0}$ [nb/GeV^4]
Q_T[GeV]

Fig.5

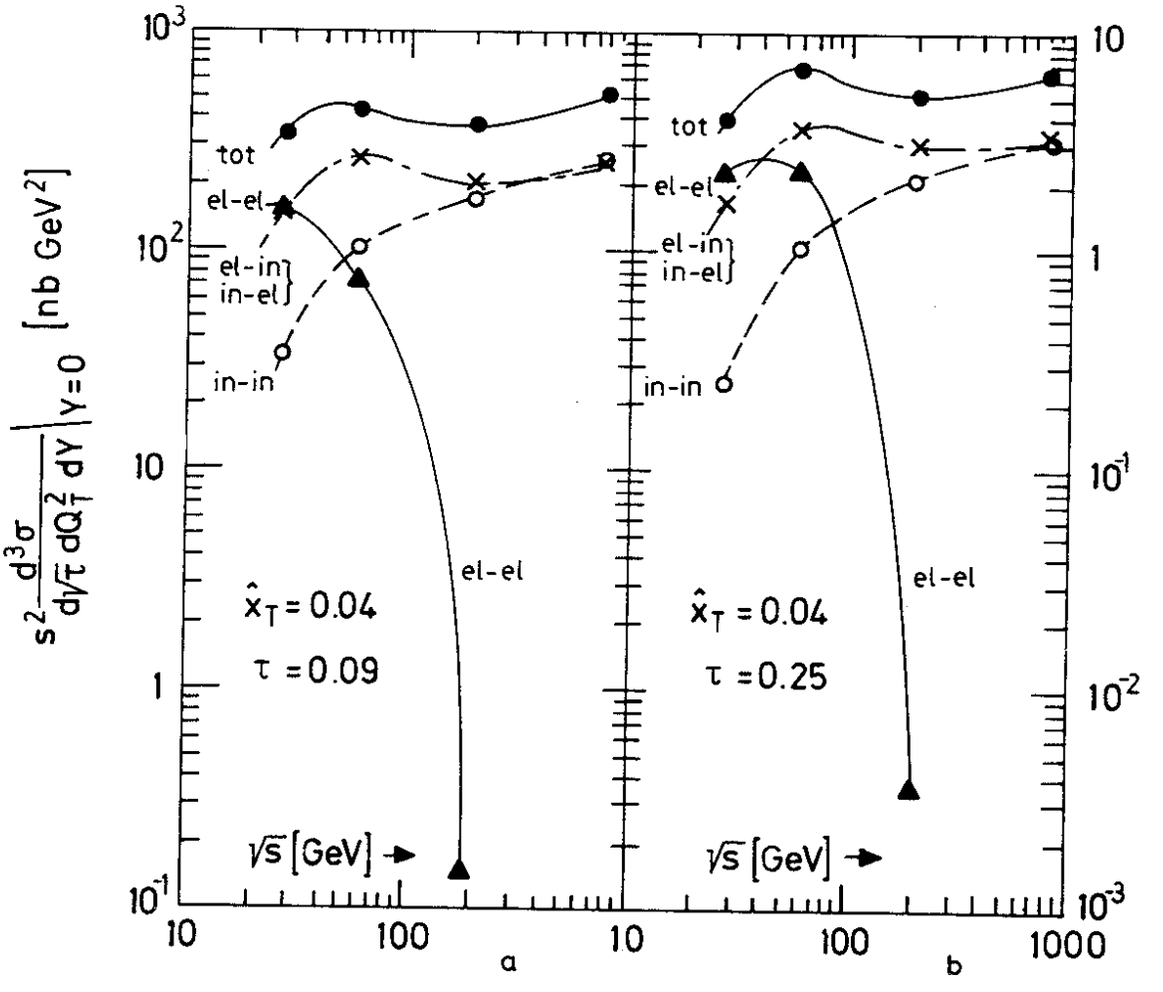
$s^2 \frac{d^3\sigma}{d\sqrt{\tau}\, dQ_T^2\, dY}\Big|_{Y=0}$ [nb GeV^2]
tot
el-el
el-in
in-el
in-in
$\hat{x}_T = 0.04$
$\tau = 0.09$
$\tau = 0.25$
$\sqrt{s}$ [GeV]
a
b

Fig.4

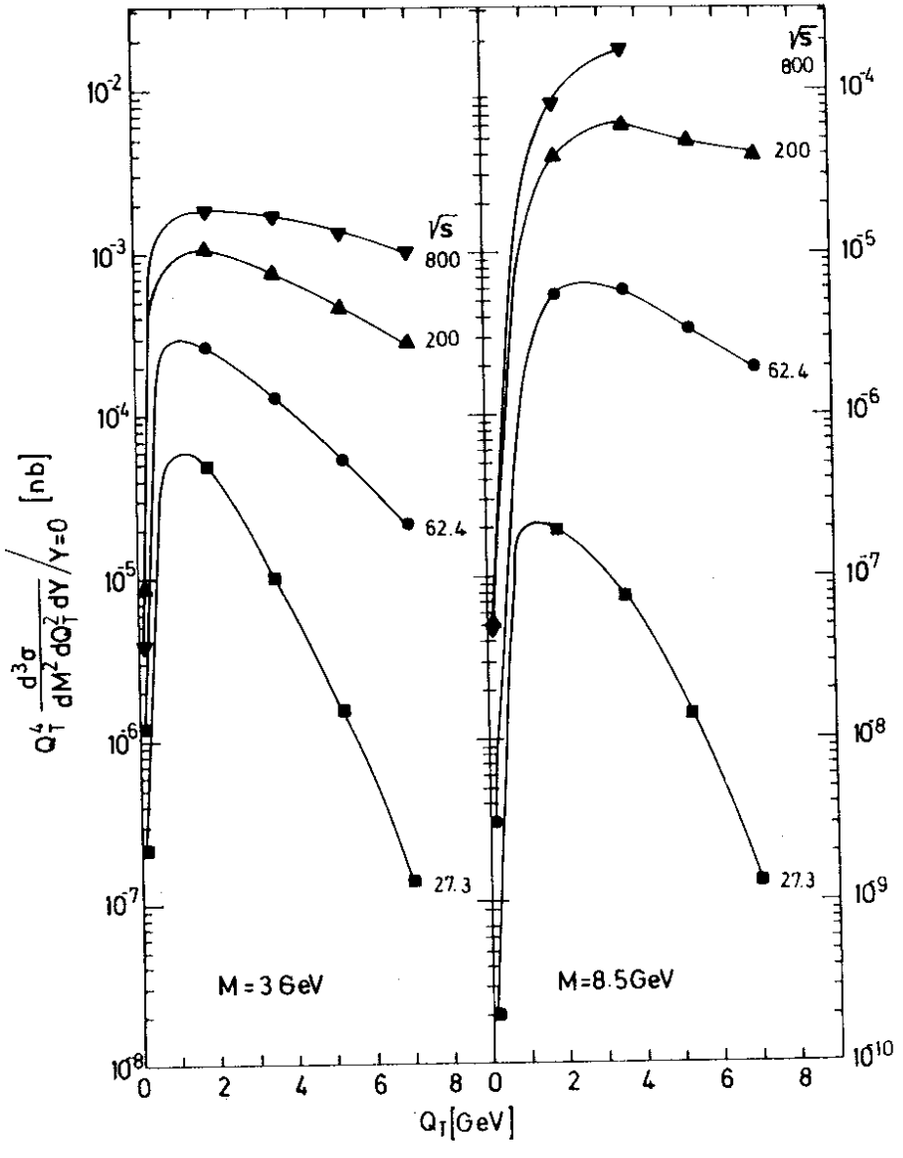
$Q_T^4 \frac{d^3\sigma}{dM^2 dQ_T^2 dY}\Big/_{Y=0}$ [nb]
Q_T[GeV]
M = 3 GeV
M = 8.5 GeV
√s
800
200
62.4
27.3

Fig.6

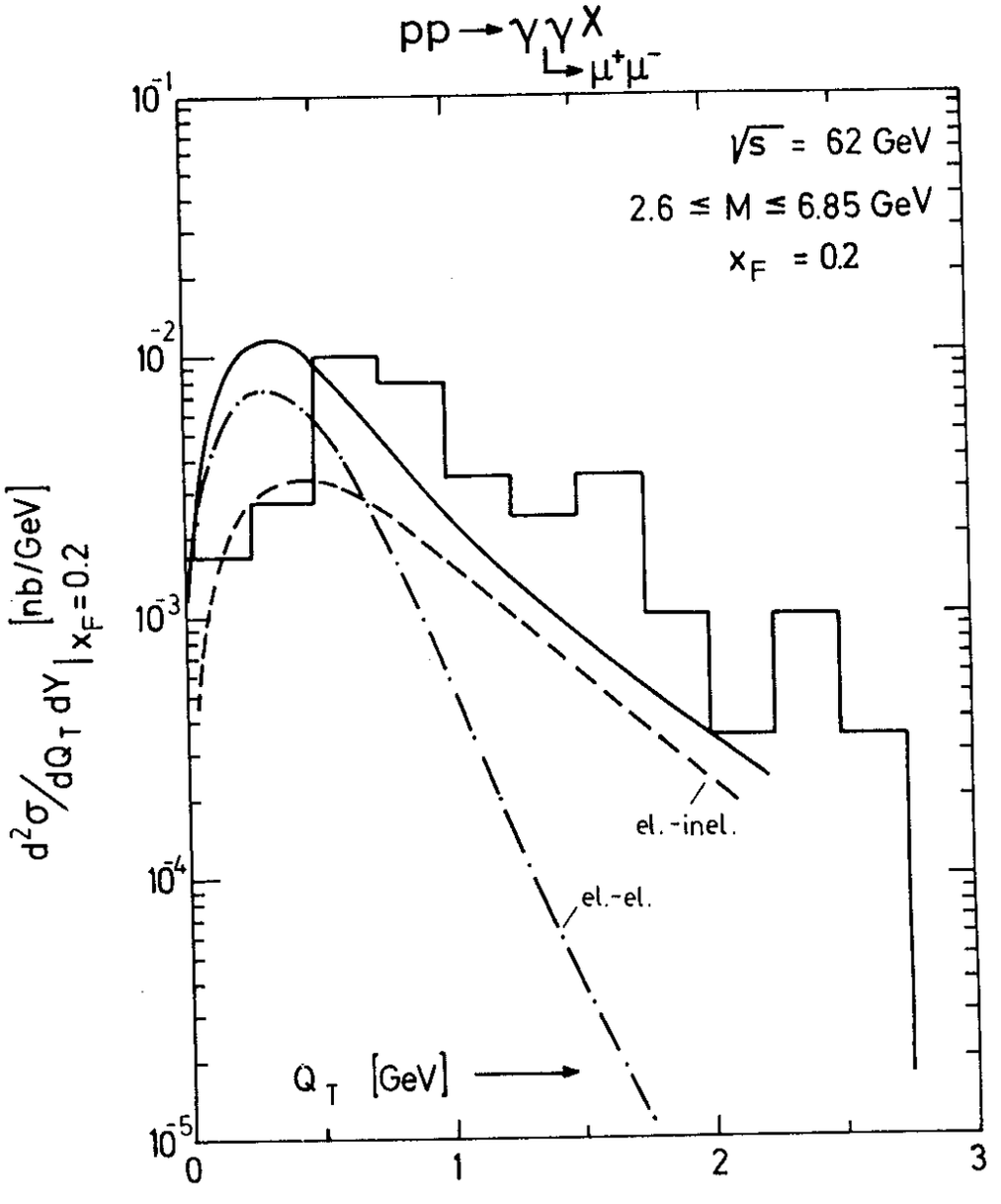
pp → γγX
↳ μ⁺μ⁻
√s = 62 GeV
2.6 ≤ M ≤ 6.85 GeV
x_F = 0.2
$d^2\sigma/dQ_T\,dY\,|_{x_F=0.2}$ [nb/GeV]
el.-inel.
el.-el.
Q_T [GeV]

Fig.7

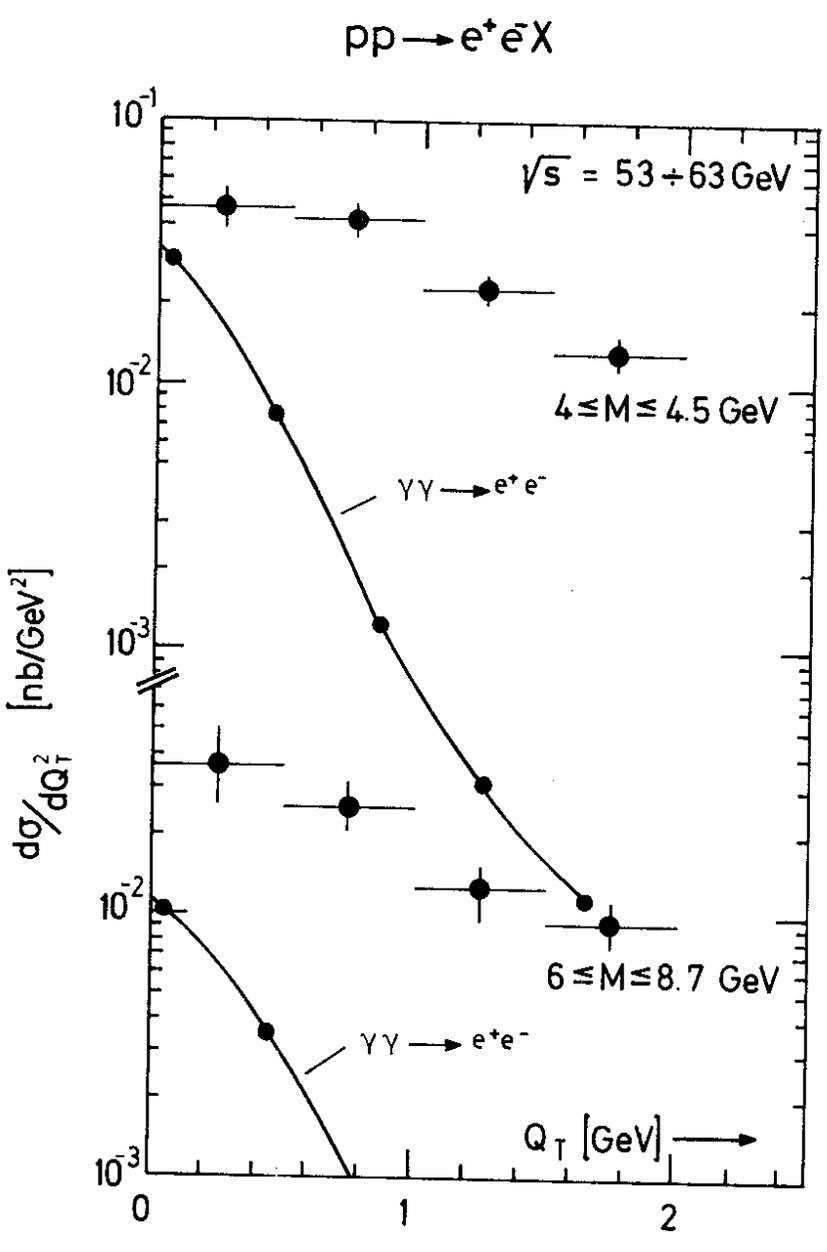
pp → e⁺e⁻X
√s = 53 ÷ 63 GeV
4 ≤ M ≤ 4.5 GeV
γγ → e⁺e⁻
6 ≤ M ≤ 8.7 GeV
γγ → e⁺e⁻
dσ/dQ_T² [nb/GeV²]
Q_T [GeV]

Fig. 8

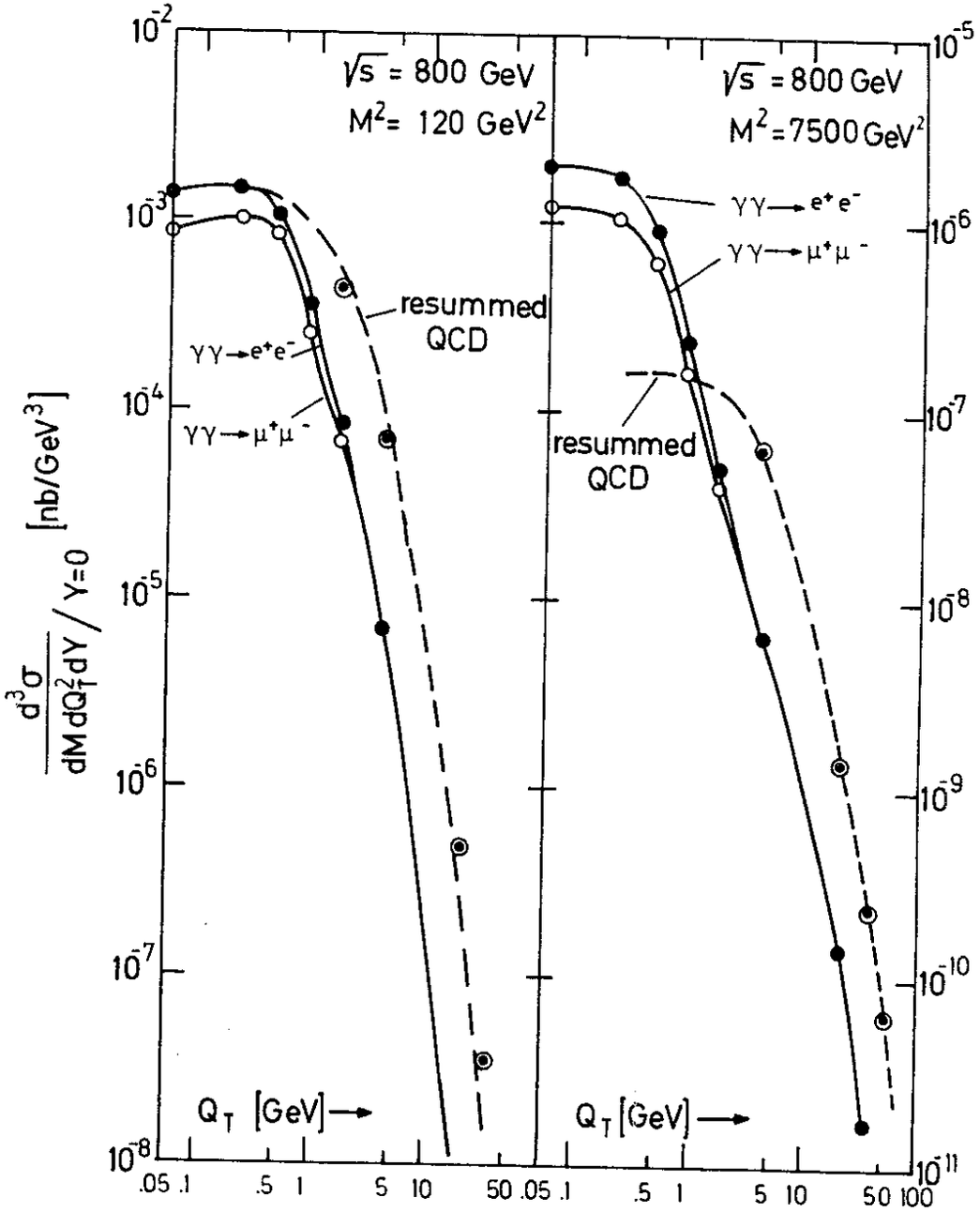
√s = 800 GeV
M² = 120 GeV²
√s = 800 GeV
M² = 7500 GeV²
γγ → e⁺e⁻
γγ → μ⁺μ⁻
resummed QCD
γγ → e⁺e⁻
γγ → μ⁺μ⁻
resummed QCD
d³σ/dM dQ_T² dY / Y=0 [nb/GeV³]
Q_T [GeV]
Q_T [GeV]

Fig. 9

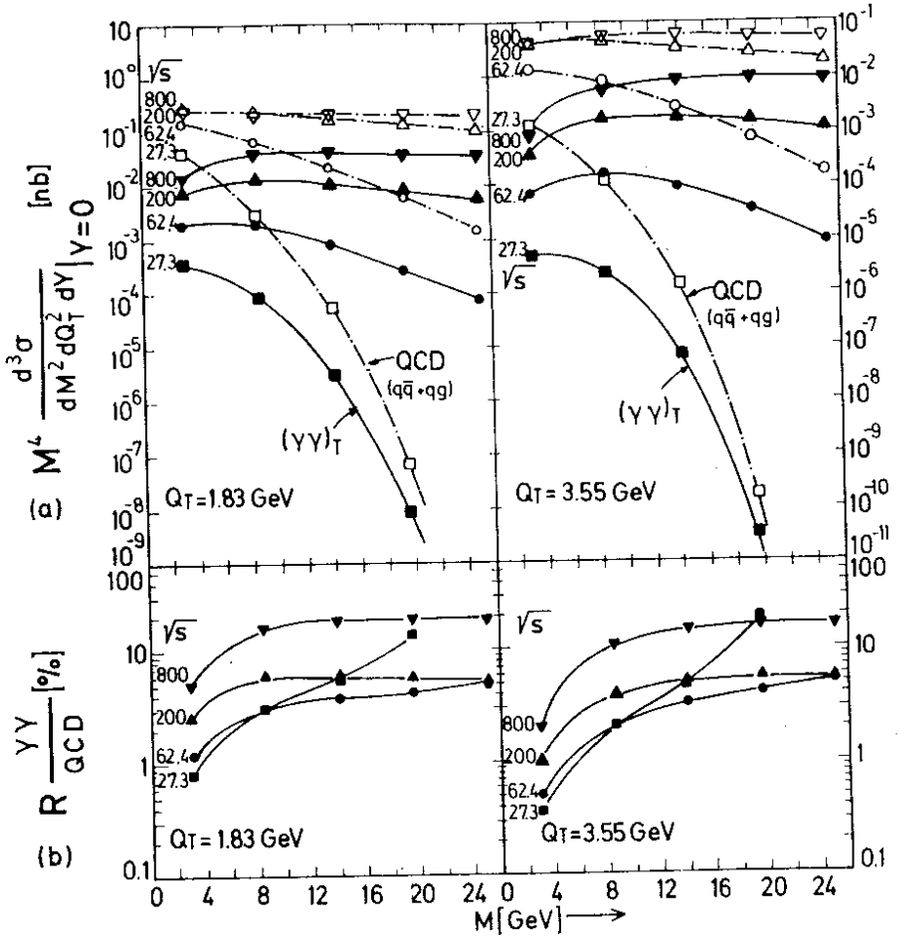
(a) $M^4 \frac{d^3\sigma}{dM^2 dQ_T^2 dY}|_{Y=0}$ [nb]
(b) $R \frac{\gamma\gamma}{QCD}$ [%]
$\sqrt{s}$
800
200
62.4
27.3
QCD ($q\bar{q}$ + qg)
$(\gamma\gamma)_T$
Q_T = 1.83 GeV
Q_T = 3.55 GeV
M [GeV] ⟶

Fig.10

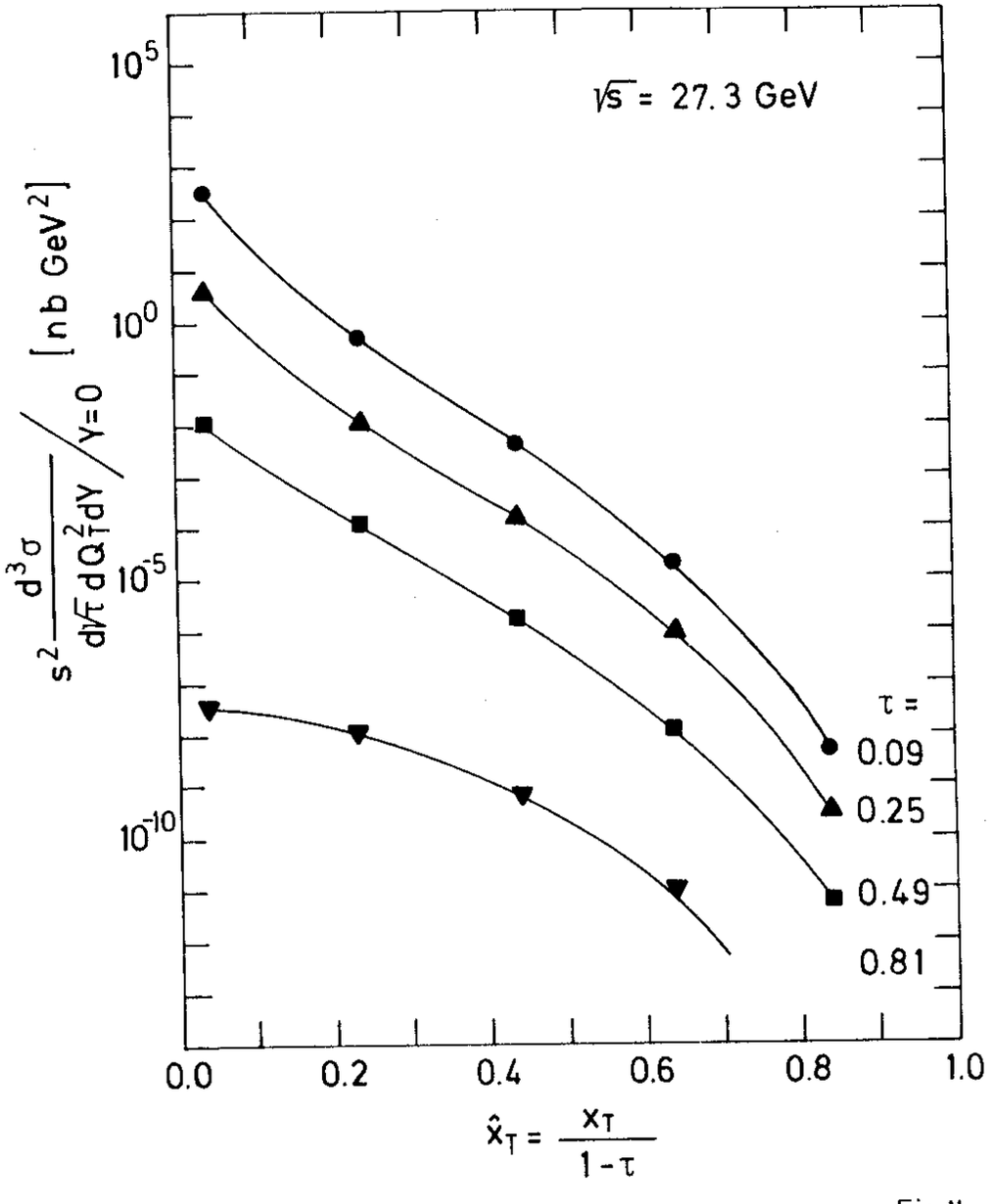
$\sqrt{s}$ = 27.3 GeV
$s^2 \frac{d^3\sigma}{d\sqrt{\tau}\, dQ_T^2 dY}|_{Y=0}$ [nb GeV^2]
$\hat{x}_T = \frac{x_T}{1-\tau}$
τ =
0.09
0.25
0.49
0.81

Fig.11

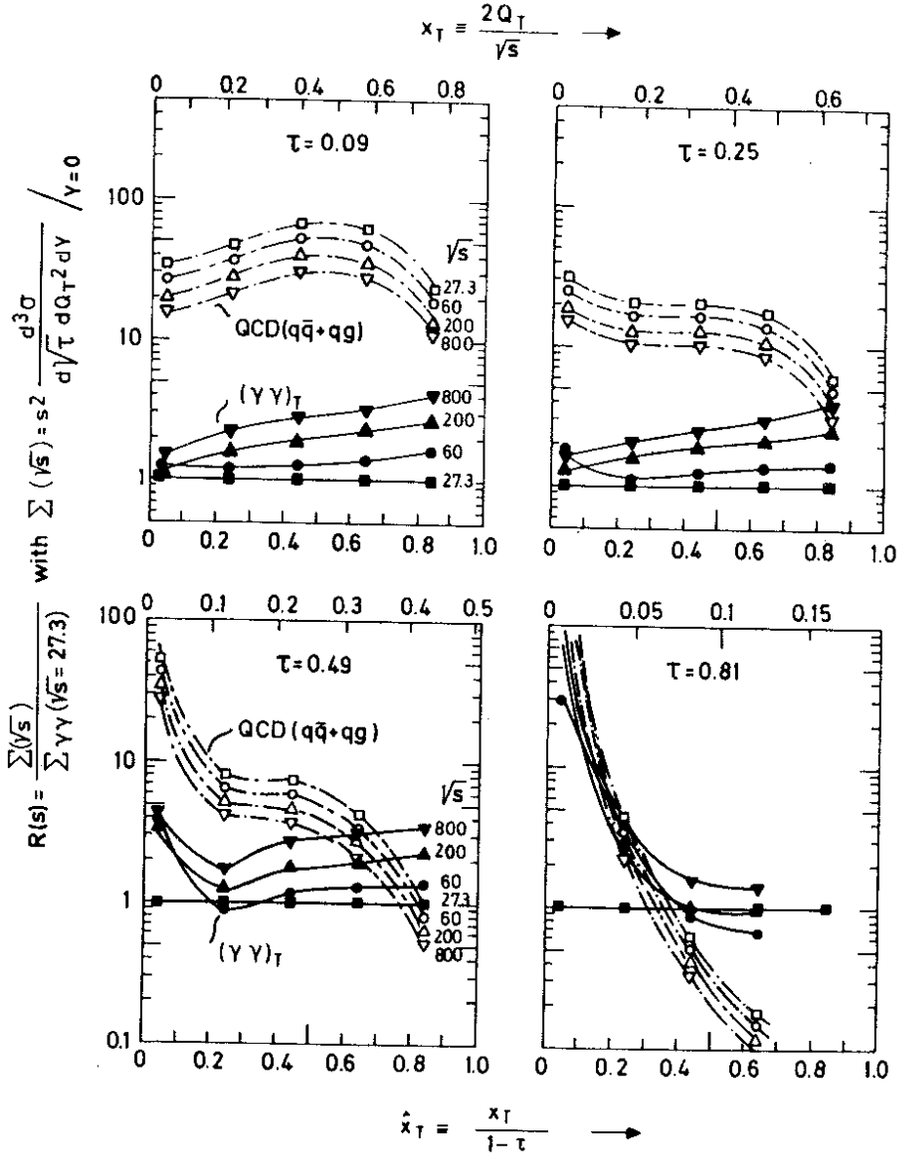
$x_T = \frac{2Q_T}{\sqrt{s}}$
$R(s) = \frac{\sum(\sqrt{s})}{\sum \gamma\gamma(\sqrt{s}=27.3)}$ with $\sum(\sqrt{s}) = s^2 \frac{d^3\sigma}{d\sqrt{\tau}\, dQ_T^2\, dY}\Big/_{Y=0}$
τ = 0.09
τ = 0.25
τ = 0.49
τ = 0.81
QCD(qq̄+qg)
$(\gamma\gamma)_T$
√s
27.3
60
200
800
$\hat{x}_T = \frac{x_T}{1-\tau}$

Fig.12

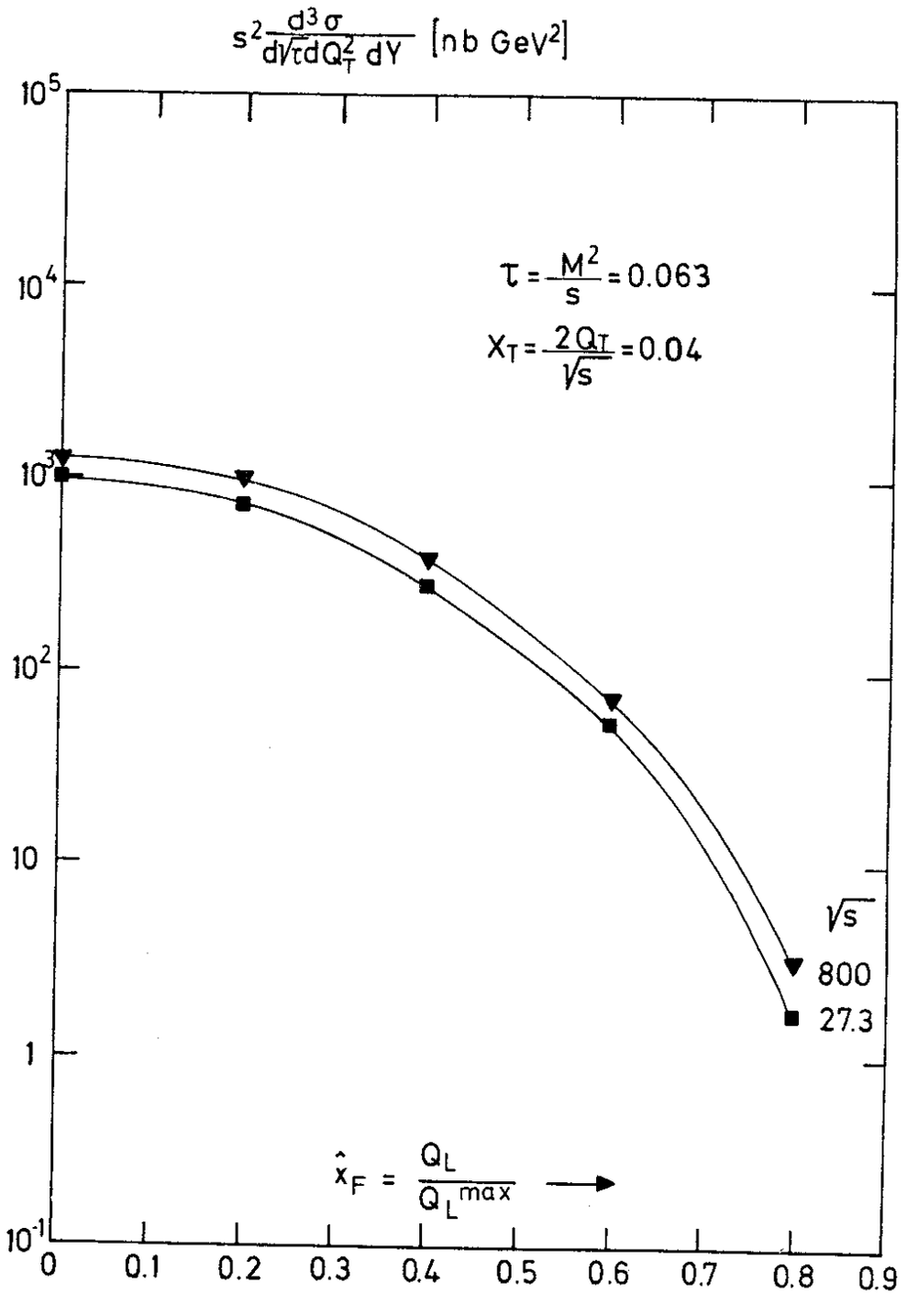
$s^2 \frac{d^3\sigma}{d\sqrt{\tau} dQ_T^2\, dY}$ [nb GeV²]
$\tau = \frac{M^2}{s} = 0.063$
$X_T = \frac{2Q_T}{\sqrt{s}} = 0.04$
√s
800
27.3
$\hat{x}_F = \frac{Q_L}{Q_L^{max}}$

Fig.13

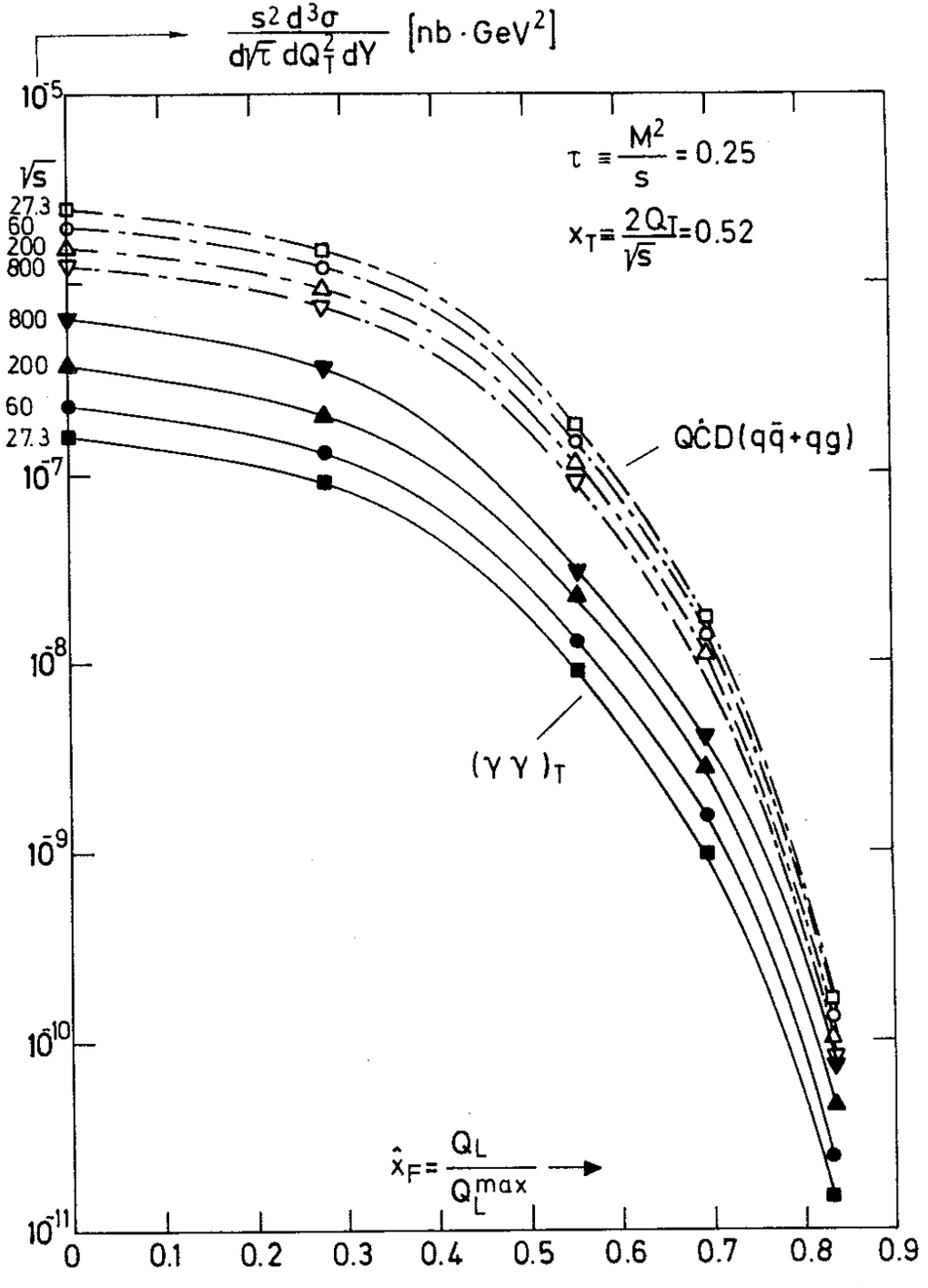
$\frac{s^2 d^3\sigma}{d\sqrt{\tau}\, dQ_T^2 dY}$ [nb · GeV^2]
$\tau \equiv \frac{M^2}{s} = 0.25$
$x_T \equiv \frac{2Q_T}{\sqrt{s}} = 0.52$
$\sqrt{s}$
27.3
60
200
800
800
200
60
27.3
QCD($q\bar{q}$+qg)
$(\gamma\gamma)_T$
$\hat{x}_F = \frac{Q_L}{Q_L^{max}}$
10^{-5}
10^{-7}
10^{-8}
10^{-9}
10^{-10}
10^{-11}
0
0.1
0.2
0.3
0.4
0.5
0.6
0.7
0.8
0.9

Fig.14